



UNIVERSITY *of the*  
WESTERN CAPE

# **Platinum Based Catalysts for the Cathode of Proton Exchange Membrane Fuel Cells**

**Linathi Ndzuzo (3341694)**

A thesis submitted in partial fulfilment of the requirements for the degree of Magister  
Scientiae in the Department of Chemistry, University of the Western Cape.

Date submitted for examination: November 2018

Supervisor: Dr Sivakumar Pasupathi

Co-supervisor: Dr Juan Carlos Calderón Gómez

## Keywords

- ✚ Pt-Pd nanoparticles
- ✚ Proton exchange membrane fuel cells
- ✚ Catalysts
- ✚ Oxygen reduction reaction
- ✚ Electrochemistry
- ✚ Carbon support
- ✚ Cathode
- ✚ Catalytic activity
- ✚ Synthesis method
- ✚ Reducing agent
- ✚ Nanoparticle dispersion



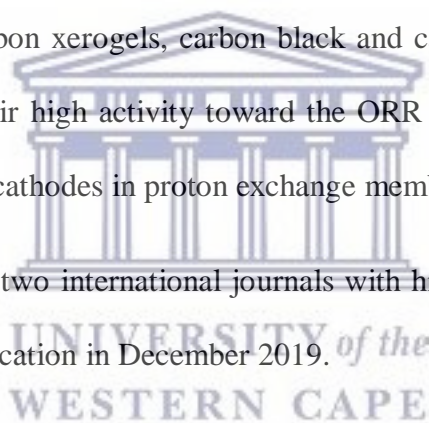
## Abstract

Oxygen reduction reaction (ORR) is carried out in the cathode of the proton exchange membrane fuel cell (PEMFC) and it is known for its sluggish kinetics and the existence of two-pathway mechanism, related with the production of water and hydrogen peroxide. Nowadays, the design of novel cathode catalysts that are able to generate both high oxygen reduction currents and water as main product is a challenge since it causes an enhancement in the performance of PEMFC. Generally, these catalysts are composed of platinum nanoparticles, bearing in mind its high activity towards the ORR. However, the use of platinum means an increase in the total cost of PEMFCs due to its scarcity and high cost. This topic has been the motivation for a wide research in the field of PEMFCs during the last several years, being the main goal to design efficient and low cost catalysts for the cathode of PEMFCs. In this Master thesis project, platinum-palladium (Pt-Pd) catalysts supported on carbon black (CB), carbon nanofibers (CNF) and carbon xerogels (CX) were synthesised using methanol (MeOH), formaldehyde (FMY), *n*-propanol (nPrOH), ethanol (EtOH) and ascorbic acid (AA). The as-prepared materials were physically characterised by energy dispersive X-ray (EDS), X-ray diffraction (XRD) and transmission electronic microscopy (TEM), in order to determine its composition and morphological characteristics. The catalytic activity towards ORR was assessed by means of electrochemical techniques as rotating disc electrode (RDE) and cyclic voltammetry (CV).

In general, Pt-Pd atomic ratios close to 1:2 were obtained, with metal contents close to 40 wt. % except in the case of the catalysts supported on carbon nanofibers. The formation of alloys between platinum and palladium was observed from the shift in the XRD typical reflections for the cubic face centred structure of platinum and the obtaining of low values for the lattice parameters, compared with the value of a commercial Pt/C catalyst. On the other hand, the

TEM analysis demonstrated a high dispersion of the nanoparticles on the carbon supports. Regarding the electrochemical characterisation, the Pt-Pd/CX-FMY, Pt-Pd/CX-MeOH, Pt-Pd/CB-AA, Pt-Pd/CB-nPrOH, Pt-Pd/CNF-EtOH and Pt-Pd/CNF-nPrOH catalysts demonstrated the highest diffusional current densities, being comparable to those obtained for Pt/C. Moreover, a Koutěcky-Levich analysis proved that most of the synthesised catalysts perform the ORR producing water as the main product, meaning that 4 electrons are involved in this reaction and therefore, the maximum performance is achieved. Remarkable corrosion resistance was observed in the catalysts supported on carbon xerogels, as they showed lower differences in the half-way potential and improved current densities after cycling treatment. The results presented here suggest that the studied synthesis routes are suitable to prepare Pt-Pd catalysts supported on carbon xerogels, carbon black and carbon nanofiber with a better use of Pt, even increasing their high activity toward the ORR and thus, making them good candidates to be employed as cathodes in proton exchange membrane fuel cells.

The results were published in two international journals with high impact factor and another article was submitted for publication in December 2019.



# Declaration

I hereby declare that, “**Platinum based catalysts for the cathode of proton exchange membrane fuel cells**” is my own work and it has not been submitted before for any degree or examination in any other university, and all the sources I have used or quoted have been indicated or acknowledged by way of complete references.

**Linathi Ndzuzo**



Signed:

Date: 10 March 2019



UNIVERSITY *of the*  
WESTERN CAPE

# Acknowledgements

I would like to humbly thank the following individuals and institutions for the help they offered in ensuring that I successfully complete my MSc research.

- ✚ Dr Sivakumar Pasupathi my supervisor, for support and making sure I have all I need for my project.
- ✚ Dr Juan Carlos Calderon Gomez my co-supervisor, for guiding my every step of the way. You literally taught me everything I know in research and thank you so much for your patience.
- ✚ iThemba Labs for XRD analysis.
- ✚ Department of Physics (UWC) for TEM and EDS analysis.
- ✚ Sasol for financial support.
- ✚ Miranda Mengwi Ndipingwi for helping me write my thesis.
- ✚ The Division for Postgraduate Studies (UWC) for workshops and writing assistance they offered throughout my MSc.
- ✚ HySA System colleagues for always offering help and support whenever needed.
- ✚ Sinombulelo Bovana for proof reading and editing the abstract.
- ✚ My family for encouragement and emotional support.
- ✚ My AOGMC “The Associates” family for support through prayers and encouragement.
- ✚ Above all else I would like to give glory to my God for strength [Philippians 4:13 NKJV] and granting me my desire [Psalms 37:4 ESV] to pursue MSc [Proverbs 16:3 CEV].

# Table of Content

## Contents

<b>Keywords</b> .....	2
<b>Abstract</b> .....	3
<b>Declaration</b> .....	5
<b>Acknowledgements</b> .....	6
<b>Table of Content</b> .....	7
<b>Acronyms and abbreviations</b> .....	10
<b>List of figures</b> .....	13
<b>List of tables</b> .....	15
<b>List of Schemes</b> .....	16
<b>1. Chapter One: Introduction</b> .....	17
1.1 Overview.....	17
1.2 Problem statement .....	19
1.3 Motivation of the study .....	20
1.4 Project aim and objectives .....	21
1.5 Research frame.....	22
1.6 Thesis outline .....	23
References .....	24
<b>2. Chapter Two: Literature Review</b> .....	28
Chapter overview .....	28
2.1 Background .....	28
2.2 Types of fuel cells .....	29
2.2.1 Alkaline fuel cells (AFCs).....	29
2.2.2 Molten Carbonate fuel cells (MCFCs).....	29
2.2.3 Phosphoric acid fuel cells (PAFCs) .....	30
2.2.4 Solid Oxide fuel cells (SOFCs) .....	30
2.2.5 Proton exchange membrane fuel cell (PEMFCs).....	30
2.3 High temperature PEMFCs .....	32
2.4 Oxygen reduction reaction .....	34
2.5 Platinum catalysts .....	36
2.6 Platinum alloys .....	37
2.7 Carbon Supports .....	37



2.7.1 Carbon Blacks.....	38
2.7.2 Carbon nanofibers.....	38
2.7.3 Carbon nanotubes .....	38
2.7.4 Carbon xerogels .....	39
References.....	40
<b>3. Chapter Three: Materials and methods</b> .....	<b>49</b>
Overview .....	49
3.1 Experimental .....	49
3.1.1 Chemicals .....	49
3.1.2 Synthesis of carbon-supported Pt-Pd nanoparticles.....	50
3.1.2.1 Synthesis using Ethanol as a reducing agent .....	50
3.1.2.2 Synthesis using Formaldehyde as a reducing agent .....	50
3.1.2.3 Synthesis using Methanol as the reducing agent.....	51
3.1.2.4 Synthesis using ascorbic acid as reducing agent.....	51
3.1.3 Characterisation techniques.....	52
3.1.3.1 Physical characterisation .....	52
3.1.3.2 Electrochemical characterisation .....	52
References.....	54
<b>4. Chapter Four: Results and Discussion</b> .....	<b>55</b>
Overview .....	55
4.1 Physical characterisation.....	55
4.1.1 Composition and particle sizes of the synthesised catalysts.....	55
4.1.1.1 Composition and particle sizes of Pt-Pd/CX .....	55
4.1.1.2 Composition and particle size of Pt-Pd/CB .....	56
4.1.1.3 Composition and particle size of Pt-Pd/CNF.....	57
4.1.1 X-Ray diffraction (XRD) characterisation of the synthesised catalysts .....	59
4.1.2 Transmission electron microscopy (TEM) characterisation of the synthesised catalysts .....	62
4.2 Electrochemical characterisation.....	65
4.2.1 Cyclic voltammetry.....	65
4.2.2 Activity towards ORR.....	69
4.2.3 Mass and specific activity of the synthesised catalysts. ....	74
4.2.4 Koutecký-Levich analysis of the synthesised catalysts.....	77
4.2.5 Corrosion and stability assessment of the synthesised catalysts.....	80
References.....	87





5. Chapter Five: Conclusions ..... 90



UNIVERSITY *of the*  
WESTERN CAPE

# Acronyms and abbreviations

- ✚ **PEMFCs**: Proton exchange membrane fuel cells.
- ✚ **ORR**: Oxygen reduction reaction
- ✚ **CX**: Carbon xerogels
- ✚ **CB**: Carbon black
- ✚ **CNF**: Carbon nanofiber
- ✚ **AA**: Ascorbic acid
- ✚ **EtOH**: Ethanol
- ✚ **FMY**: Formaldehyde
- ✚ **MeOH**: Methanol
- ✚ **nPrOH**: Propanol
- ✚ **CV**: Cyclic voltammetry
- ✚ **RDE**: Rotating disc electrode
- ✚ **EDS**: Energy dispersive X-ray
- ✚ **XRD**: X-Ray diffraction
- ✚ **TEM**: Transmission electron microscopy
- ✚ **DMFCs**: Direct methanol fuel cells
- ✚ **AFCs**: Alkaline fuel cells
- ✚ **SOFCs**: Solid oxide fuel cells
- ✚ **MCFCs**: Molten carbonate fuel cells
- ✚ **RFCs**: Reversible fuel cells
- ✚ **Pt-Pd/CX-AA**: Platinum-Palladium catalyst supported on carbon xerogel, reduced with ascorbic acid.



- ✚ **Pt-Pd/CX-EtOH:** Platinum-Palladium catalyst supported on carbon xerogel, reduced with ethanol.
- ✚ **Pt-Pd/CX-FMY:** Platinum-Palladium catalyst supported on carbon xerogel, reduced with formaldehyde.
- ✚ **Pt-Pd/CX-MeOH:** Platinum-Palladium catalyst supported on carbon xerogel, reduced with methanol.
- ✚ **Pt-Pd/CX-nPrOH:** Platinum-Palladium catalyst supported on carbon xerogel, reduced with propanol.
- ✚ **Pt-Pd/CB-AA:** Platinum-Palladium catalyst supported on carbon black, reduced with ascorbic acid.
- ✚ **Pt-Pd/CB-EtOH:** Platinum-Palladium catalyst supported on carbon black, reduced with ethanol.
- ✚ **Pt-Pd/CB-FMY:** Platinum-Palladium catalyst supported on carbon black, reduced with formaldehyde.
- ✚ **Pt-Pd/CB-MeOH:** Platinum-Palladium catalyst supported on carbon black, reduced with methanol.
- ✚ **Pt-Pd/CB-nPrOH:** Platinum-Palladium catalyst supported on carbon black, reduced with propanol.
- ✚ **Pt-Pd/CNF-AA:** Platinum-Palladium catalyst supported on carbon nanofiber, reduced with ascorbic acid.
- ✚ **Pt-Pd/CNF-EtOH:** Platinum-Palladium catalyst supported on carbon nanofiber, reduced with ethanol.
- ✚ **Pt-Pd/CNF-FMY:** Platinum-Palladium catalyst supported on carbon nanofiber, reduced with formaldehyde.



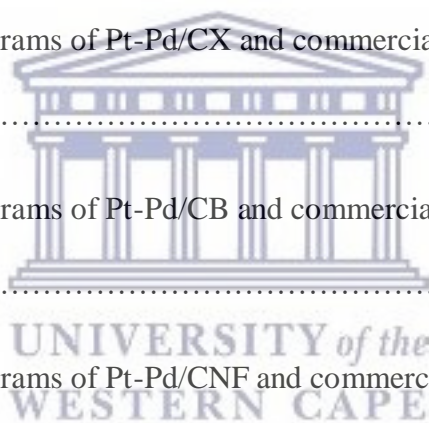
- ✚ **Pt-Pd/CNF-MeOH**: Platinum-Palladium catalyst supported on carbon nanofiber, reduced with methanol.
- ✚ **Pt-Pd/CNF-nPrOH**: Platinum-Palladium catalyst supported on carbon nanofiber, reduced with propanol.
- ✚ **Pt/C Alfa Aesar**: Platinum catalyst supported on carbon from Alfa Aesar.



## List of figures

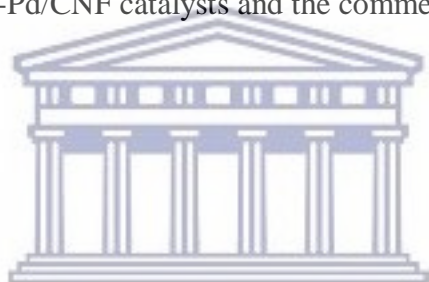
Figure 4.1 XRD patterns of synthesised Pt-Pd/CX and the commercial catalyst.....	60
Figure 4.2 XRD patterns of synthesised Pt-Pt/CB and the commercial catalyst.....	61
Figure 4.3 XRD patterns of synthesised Pt-Pt/CNF and the commercial catalyst.....	62
Figure 4.4 TEM images and histograms of Pt-Pd/CX and commercial Pt/C from Alfa Aesar.....	63
Figure 4.5 TEM images and histograms of Pt-Pd/CB and commercial Pt/C from Alfa Aesar.....	64
Figure 4.6 TEM images and histograms of Pt-Pd/CNF and commercial Pt/C from Alfa Aesar.....	65
Figure 4.7 Cyclic voltammograms of the synthesised Pt-Pd/CX and commercial Pt/C in the supporting electrolyte (0.1 M HClO <sub>4</sub> ). Scan rate 20mVs <sup>-1</sup> .....	66
Figure 4.8 Cyclic voltammograms of the synthesised Pt-Pd/CB and commercial Pt/C in the supporting electrolyte (0.1 M HClO <sub>4</sub> ). Scan rate 20mVs <sup>-1</sup> .....	67
Figure 4.9 Cyclic voltammograms of the synthesised Pt-Pd/CNF and commercial Pt/C in the supporting electrolyte (0.1 M HClO <sub>4</sub> ). Scan rate 20mVs <sup>-1</sup> .....	68
Figure 4.10 Activity of the synthesised Pt-Pd/CX catalysts and commercial Pt/C towards ORR.....	71
Figure 4.11 Activity of the synthesised Pt-Pd/CB catalysts and commercial Pt/C towards ORR.....	73

Figure 4.12 Activity of the synthesised Pt-Pd/CNF catalysts and commercial Pt/C towards ORR.....	74
Figure 4.13 Specific and mass activity of Pt-Pd/CX catalysts and commercial Pt/C.....	75
Figure 4.14 Specific and mass activity of Pt-Pd/CB catalysts and commercial Pt/C.....	76
Figure 4.15 Specific and mass activity of Pt-Pd/CNF catalysts and commercial Pt/C.....	77
Figure 4.16 Koutecky-Levich plots of the Pt-Pd/CX and commercial Pt/C.....	78
Figure 4.17 Koutecky-Levich plots of the Pt-Pd/CB and commercial Pt/C.....	79
Figure 4.18 Koutecky-Levich plots of the Pt-Pd/CNF and commercial Pt/C.....	80
Figure 4.19 Cyclic voltammograms of Pt-Pd/CX and commercial Pt/C before and after durability test.....	81
Figure 4.20 Cyclic voltammograms of Pt-Pd/CB and commercial Pt/C before and after durability test.....	82
Figure 4.21 Cyclic voltammograms of Pt-Pd/CNF and commercial Pt/C before and after durability test.....	83
Figure 4.22 ORR linear sweep voltammograms of Pt-Pd/CX and commercial catalysts before and after durability test.....	84
Figure 4.23 ORR linear sweep voltammograms of Pt-Pd/CB and commercial catalysts before and after durability test.....	85
Figure 4.24 ORR linear sweep voltammograms of Pt-Pd/CNF and commercial catalysts before and after durability test.....	86



## List of tables

Table 4.1 Physical characterisation of Pt-Pd/CX catalysts.....	56
Table 4.2 Physical characterisation of Pt-Pd/CB catalysts.....	57
Table 4.3 Physical characterisation of Pt-Pd/CNF catalysts.....	58
Table 4.4 Electrochemical surface area of the synthesised catalysts.....	69
Table 4.5 ORR activities of Pt-Pd/CX catalysts and the commercial catalyst.....	70
Table 4.6 ORR activities of Pt-Pd/CB catalysts and the commercial catalyst.....	72
Table 4.7 ORR activities of Pt-Pd/CNF catalysts and the commercial catalyst.....	73



UNIVERSITY *of the*  
WESTERN CAPE

# List of Schemes

1.1 Scheme of a PEMFC.....	18
1.2 Research frame.....	22
2.1 Scheme of a PEMFC (components and involved reactions).....	31
2.2 Schematic representation of total reduction of oxygen.....	35
2.3 Schematic representation of partial reduction of oxygen.....	36



UNIVERSITY *of the*  
WESTERN CAPE



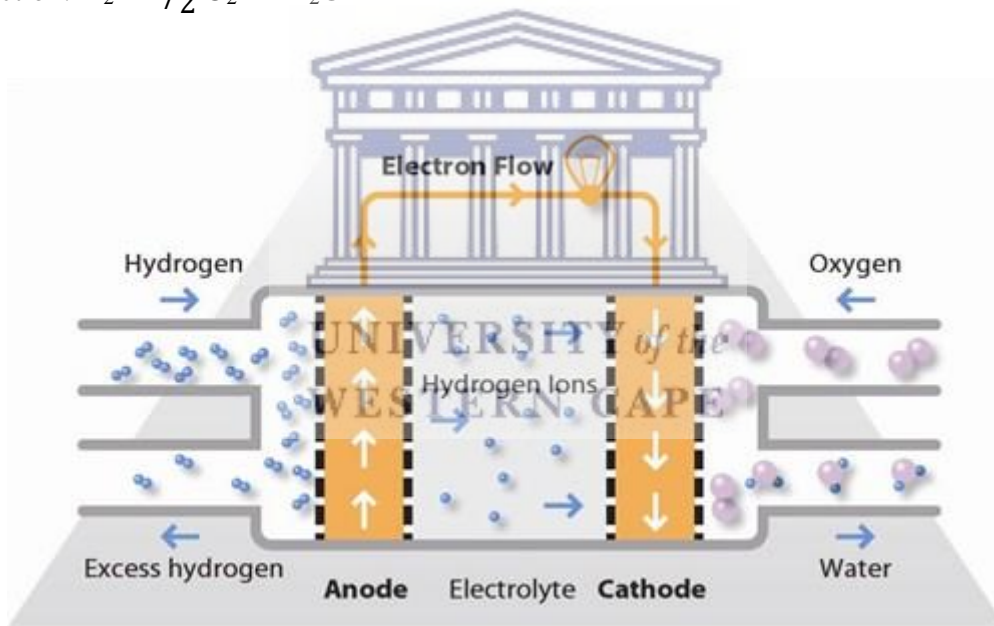
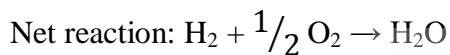
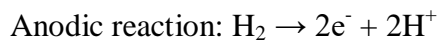
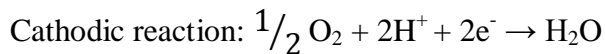
# 1. Chapter One: Introduction

## 1.1 Overview

Sustainable energy generation and conversion is a widely discussed topic by the society due to the enhanced deterioration of the natural environment and the evident depletion of fossil fuels. In order to perform the conversion of more clean fuels such as hydrogen, methanol or formic acid to electricity, which produce less contaminant residues, fuel cells have been considered as alternative to supply the current energy demand [1]. Fuel cells use oxygen and hydrogen as reactants to produce water as product which is not harmful to the environment. A lot of research and development has been devoted on different types of fuel cells [2, 3] which include: (1) direct methanol fuel cells (DMFCs) [4] that use methanol fuel which is oxidised to carbon dioxide to form water; (2) alkaline fuel cells (AFCs) [5], operating with compressed hydrogen and oxygen and a potassium hydroxide solution in water as electrolyte; (3) molten carbonate fuel cells (MCFCs) [6], employing molten sodium or magnesium carbonates as electrolyte; (4) solid oxide fuel cells (SOFCs) [7] that are conformed by a ceramic calcium or zirconium oxide playing the role of interface between the electrodes; (5) reversible fuel cell (RFC) have a first electrode and a second electrode separated by an ionically conducting electrolyte, and at least two chambers adapted to hold fuel (preferably hydrogen and oxygen) and each chamber being in passive communication with the fuel cell, wherein the system is substantially closed [8]; (6) phosphoric acid fuel cell (PAFC) consists of an anode and a cathode made of a finely dispersed platinum; they use phosphoric acid as an electrolyte [9]; and finally (7) proton exchange membrane fuel cells (PEMFCs) [10], where a polymer membrane acts as electrolyte.

Regarding the proton exchange membrane fuel cells (PEMFCs), they have attracted a lot of attention because of their advantages such as low operating temperature, low pollutant

emission, sustained operation at high current density, low weight and volume, compactness, long stack life, fast start-ups and sustainability for discontinues operations [3, 10, 11]. In the PEMFC, hydrogen is oxidised in the anode to produce electrons and protons. The electrons go through the electrical circuit while the protons pass through the proton exchange membrane to the cathode to combine with the fed oxygen forming water. These are the reactions associated with this process:



*Scheme 1.1: Scheme of a proton exchange membrane fuel cell [12]*

Traditionally, PEMFCs possess platinum (Pt) catalysts in both the cathode and the anode to perform the mentioned reactions. Nonetheless, in spite of the promising achievements and plausible prospects of PEMFCs, there are still some problems associated to these devices such as the high cost of platinum used as catalyst, low durability and sluggish kinetics, the requirement of very pure hydrogen (with much lower than 5 ppm CO), which is typically

produced via steam reforming or partial oxidation of natural gas, methanol, or other liquid fuels, which hinder their successful commercialisation [13-17].

In order to obtain a catalyst with high activity, the content of Pt should decrease while the ORR performance is increased [18]. The use of Pt alloyed with metals such as palladium (Pd) has enhanced the kinetics of the ORR, reducing the production of hydrogen peroxide as collateral product [19]. This is due to the fact that Pd has high activity towards ORR in an acidic medium, being a good alternative to partially replace Pt as catalyst in the cathode of PEMFCs. The entrance of Pd into the crystallographic structure of Pt decreases the Pt-Pt interatomic distance, facilitating the oxygen adsorption on the nanoparticle surface [20, 21]. Besides the mentioned facts, South Africa possesses more than 75% of the platinum group metal (PGM) world reserves, making indispensable the development of PGM-based components for proton exchange membrane fuel cells and other technologies to produce clean renewable energy, in line with the national strategy to use the country's natural resources [22]. Bimetallic alloys supported on carbon supports have also been reported to have an enhanced effect on ORR performance. This is due to the fact that carbon supports have high surface area, high chemical and electrochemical stability, good porous size and high conductivity [23]. The most commonly used carbon supports are carbon blacks, carbon nanofibers and carbon nanotubes [24-26] Based on the above mentioned facts, Pt-Pd alloys supported on carbon structures are promising candidates to be used as catalysts for the ORR in the cathode of PEMFCs.

## 1.2 Problem statement

Oxygen reduction reaction (ORR) occurs on the cathode of proton exchange membrane fuel cells (PEMFC), being addressed by a reaction mechanism with two pathways: the direct 4-electron reduction pathway, from  $O_2$  to  $H_2O$ , and the 2-electron reduction pathway, from  $O_2$

to hydrogen peroxide (H<sub>2</sub>O<sub>2</sub>) [27]. The water pathway is the most efficient route, involving the maximum number of transferred electrons (4) and the production of water as residue, resulting in less corrosion for the PEMFC components. The kinetics associated to ORR is very slow, thus the use of a catalyst with high activity to perform this reaction is crucial, being the platinum-based catalysts the most employed materials for this purpose. Nevertheless, due to several factors as high cost of Pt, limited adsorption of oxygen on Pt caused by oxides and the partial increase of reaction rates, extensive research has focused their efforts in developing alternative catalysts with low or zero content of Pt and high catalytic activities. These options include macrocyclic compounds [28], chalcogenides, carbides [27] and alloys between Pt and transition metals. Particularly, Pt alloys have demonstrated a suitable performance when used as cathodes, due to some effects caused by the insertion of second metal such as reduction of surface Pt oxides, reduction of Pt-Pt distance and increase in the resistance to corrosion [29]. Other important research line is the design of novel carbon materials with improved morphological and electrical properties, which can be able to support and increase the catalytic activity of metal nanoparticles through high dispersion of them and particle sizes limited to a small range of diameters [20].

### 1.3 Motivation of the study

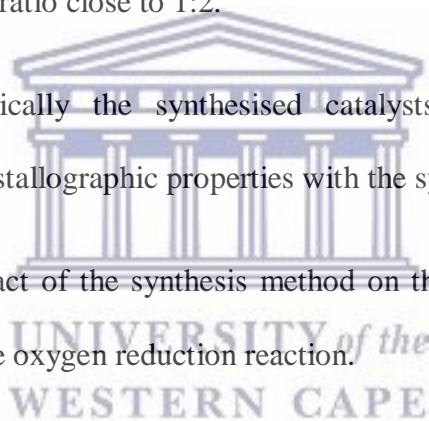
Considering the previously exposed drawbacks of oxygen reduction reaction in PEMFC, it is necessary to design novel Pt catalysts alloyed with transition metals and supported on different carbon materials such as carbon black, carbon nanofibers and carbon xerogels. Carbon supports have been reported to have unique characteristic such as high surface area, good pore size and high conductivity and they have been widely used for electrochemical applications. These catalysts can enhance the performance of cathodes toward the ORR,

producing less amounts of hydrogen peroxide, increasing the ORR kinetics and decreasing the content of Pt.

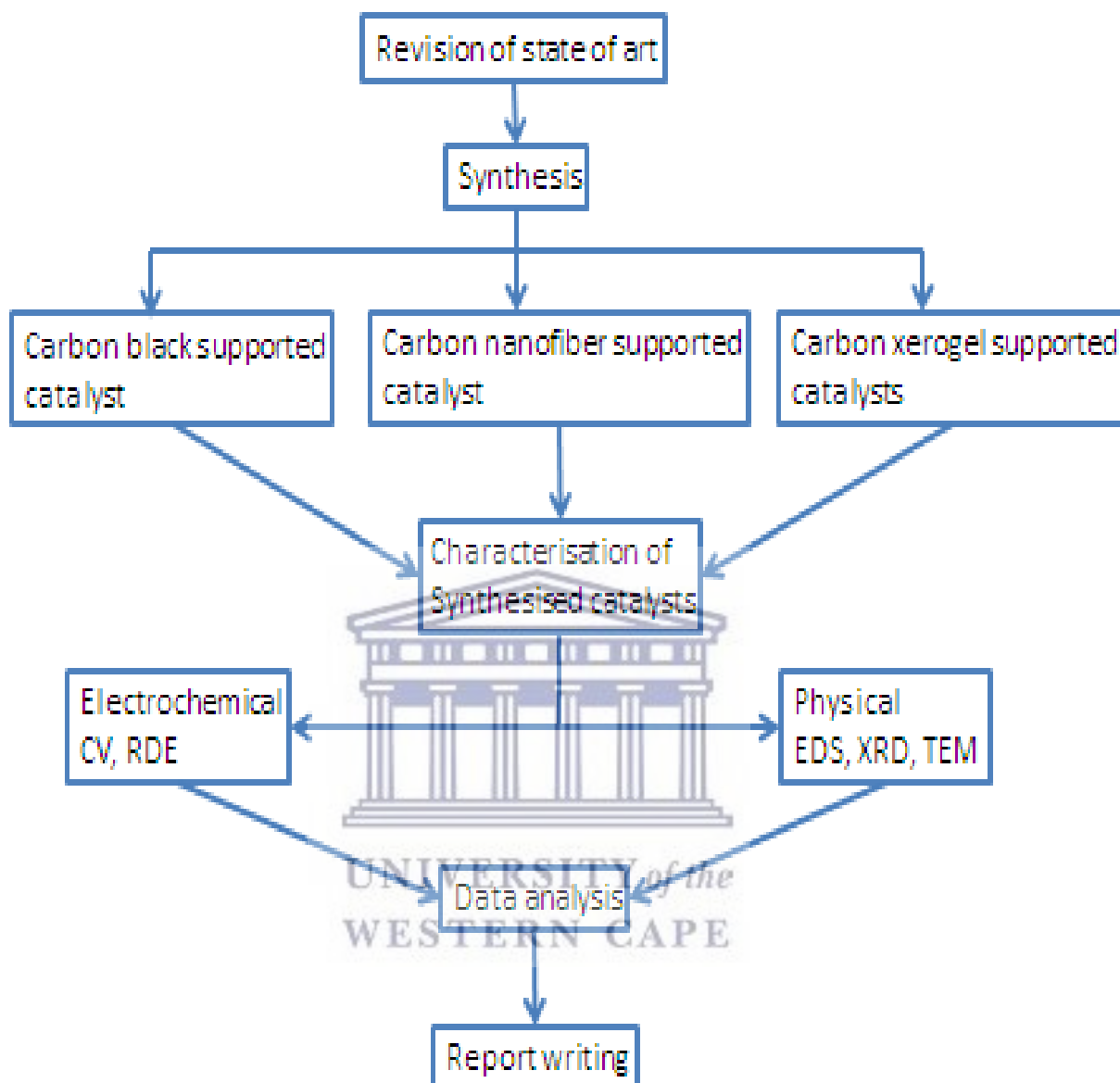
## 1.4 Project aim and objectives

The aim of this project is to design an efficient catalyst for the oxygen reduction reaction in the cathode of PEMFCs, using Pt-Pd alloyed nanoparticles supported on various carbon supports. The research is based on the following objectives:

- To design different synthesis routes for the preparation of Pt-Pd catalyst supported on carbon blacks, carbon nanofibers and carbon xerogels with metal content close to 40 wt% and Pt-Pd atomic ratio close to 1:2.
- To characterise physically the synthesised catalysts in order to correlate its morphological and crystallographic properties with the synthesis method.
- To determine the impact of the synthesis method on the electrochemical activity of the catalyst towards the oxygen reduction reaction.
- To assess the corrosion resistance of the materials and the influence of the synthesis method.



## 1.5 Research frame



*Scheme 1.2 Scheme of the research frame.*

## 1.6 Thesis outline

The thesis will be divided into four chapters which are the following:

- Chapter 1 provides an overview on the current state of proton exchange membrane fuel cells and the objectives of the study.
- Chapter 2 is the literature review of proton exchange membrane fuel cells in general, the current state of oxygen reduction reaction in these devices and the use of platinum-based alloys to perform the ORR.
- Chapter 3 describes the experimental synthesis methods and characterisation techniques used in this study.
- Chapter 4 discusses the data obtained from the physical characterisation; including the X-ray diffraction (XRD), transmission electron microscopy (TEM) and energy dispersive X-ray (EDX) as well as the electrochemical characterisation and the activity towards the oxygen reduction reaction of the carbon supported Pt-Pd nanoparticles obtained by cyclic voltammetry (CV) and rotating disc electrode (RDE).
- Chapter 5 draws a conclusion based on the outcomes of the researched compared with the already-existing literature.

## References

1. Nitze, F., 2013. Synthesis and characterization of palladium based carbon nanostructure-composites and their clean-energy application (Doctoral dissertation, Umeå University). [accessed online, 26 February 2017]
2. Park, J.H., Sohn, Y., Kim, P. and Joo, J.B., 2016. Pt deposited Pt–Pd/C electrocatalysts with the enhanced oxygen reduction activity. *Journal of Industrial and Engineering Chemistry*, 36, pp.109-115.
3. Wee, J.H., 2007. Applications of proton exchange membrane fuel cell systems. *Renewable and sustainable energy reviews*, 11(8), pp.1720-1738.
4. Liu, H., Song, C., Zhang, L., Zhang, J., Wang, H. and Wilkinson, D.P., 2006. A review of anode catalysis in the direct methanol fuel cell. *Journal of Power Sources*, 155(2), pp.95-110.
5. Coutanceau, C., Demarconnay, L., Lamy, C. and Léger, J.M., 2006. Development of electrocatalysts for solid alkaline fuel cell (SAFC). *Journal of Power Sources*, 156(1), pp.14-19.
6. Dicks, A.L., 2004. Molten carbonate fuel cells. *Current Opinion in Solid State and Materials Science*, 8(5), pp.379-383.
7. Singhal, S.C., 2007. Solid oxide fuel cells. *The Electrochemical Society Interface*, 16(4), p.41.
8. Irvine, J.T.S., Nairn, J.M., Conner, P.A., Rennie, J., Feighery, A., Jones, F.G.E., Eccleston, K.L. and Attidekou, P.S., University of St Andrews, 2014. *Reversible fuel cell*. U.S. Patent 8,748,052.



9. Lucia, U., 2014. Overview on fuel cells. *Renewable and Sustainable Energy Reviews*, 30, pp.164-169.
10. Steele, B.C. and Heinzl, A., 2011. Materials for fuel-cell technologies. In *Materials For Sustainable Energy: A Collection of Peer-Reviewed Research and Review Articles from Nature Publishing Group* (pp. 224-231).
11. Jacobson, M.Z., Colella, W.G. and Golden, D.M., 2005. Cleaning the air and improving health with hydrogen fuel-cell vehicles. *Science*, 308(5730), pp.1901-1905.
12. Johnson Matthey 2018, FuelCellToday, accessed 22 March 2018, <http://www.fuelcelltoday.com/technologies/pemfc>
13. Mehta, V. and Cooper, J.S., 2003. Review and analysis of PEM fuel cell design and manufacturing. *Journal of Power Sources*, 114(1), pp.32-53.
14. Wu, J., Yuan, X.Z., Martin, J.J., Wang, H., Zhang, J., Shen, J., Wu, S. and Merida, W., 2008. A review of PEM fuel cell durability: Degradation mechanisms and mitigation strategies. *Journal of Power Sources*, 184(1), pp.104-119.
15. Kadirgan, F., Kannan, A.M., Atilan, T., Beyhan, S., Ozenler, S.S., Suzer, S. and Yörür, A., 2009. Carbon supported nano-sized Pt–Pd and Pt–Co electrocatalysts for proton exchange membrane fuel cells. *International journal of hydrogen energy*, 34(23), pp.9450-9460.
16. Zhou, Z.M., Shao, Z.G., Qin, X.P., Chen, X.G., Wei, Z.D. and Yi, B.L., 2010. Durability study of Pt–Pd/C as PEMFC cathode catalyst. *International journal of hydrogen energy*, 35(4), pp.1719-1726.

17. Kadirgan, F., Kannan, A.M., Atilan, T., Beyhan, S., Ozenler, S.S., Suzer, S. and Yörür, A., 2009. Carbon supported nano-sized Pt–Pd and Pt–Co electrocatalysts for proton exchange membrane fuel cells. *International journal of hydrogen energy*, 34(23), pp.9450-9460.
18. Zheng, Y., Qiao, J., Yuan, J., Shen, J., Wang, A.J. and Gong, P., 2018. One-pot synthesis of PtPd dendritic nano-cube cage superstructure on graphenes as advanced catalysts for oxygen reduction. *Nanotechnology*.
19. Zhou, Z.M., Shao, Z.G., Qin, X.P., Chen, X.G., Wei, Z.D. and Yi, B.L., 2010. Durability study of Pt–Pd/C as PEMFC cathode catalyst. *International journal of hydrogen energy*, 35(4), pp.1719-1726.
20. Calderón, J.C., Ndzuzo, L., Bladergroen, B.J. and Pasupathi, S., 2018. Oxygen reduction reaction on Pt-Pd catalysts supported on carbon xerogels: Effect of the synthesis method. *International Journal of Hydrogen Energy*.
21. Maghsodi, A., Hoseini, M.M., Mobarakeh, M.D., Kheirmand, M., Samiee, L., Shoghi, F. and Kameli, M., 2011. Exploration of bimetallic Pt-Pd/C nanoparticles as an electrocatalyst for oxygen reduction reaction. *Applied Surface Science*, 257(15), pp.6353-6357.
22. Pollet, B.G., Pasupathi, S., Swart, G., Mouton, K., Lototskyy, M., Williams, M., Bujlo, P., Ji, S., Bladergroen, B.J. and Linkov, V., 2014. Hydrogen South Africa (HySA) systems competence centre: mission, objectives, technological achievements and breakthroughs. *International journal of hydrogen energy*, 39(8), pp.3577-3596.
23. Du, L., Shao, Y., Sun, J., Yin, G., Liu, J. and Wang, Y., 2016. Advanced catalyst supports for PEM fuel cell cathodes. *Nano Energy*, 29, pp.314-322.

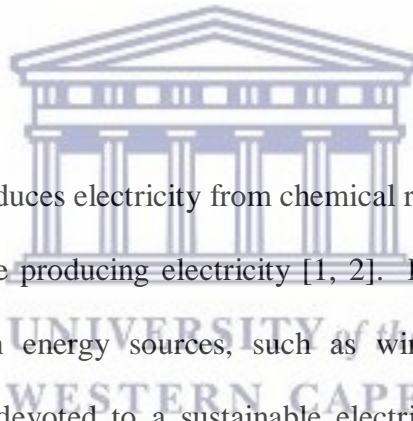
24. Trogadas, P., Fuller, T.F. and Strasser, P., 2014. Carbon as catalyst and support for electrochemical energy conversion. *Carbon*, 75, pp.5-42.
25. Wang, Y.J., Fang, B., Li, H., Bi, X.T. and Wang, H., 2016. Progress in modified carbon support materials for Pt and Pt-alloy cathode catalysts in polymer electrolyte membrane fuel cells. *Progress in Materials Science*, 82, pp.445-498.
26. Sharma, S. and Pollet, B.G., 2012. Support materials for PEMFC and DMFC electrocatalysts—a review. *Journal of Power Sources*, 208, pp.96-119.
27. Zhang, J., Shuihua, T.A.N.G., Longyu, L.I.A.O. and Weifei, Y.U., 2013. Progress in non-platinum catalysts with applications in low temperature fuel cells. *Chinese Journal of Catalysis*, 34(6), pp.1051-1065.
28. Wang, Z.B., Yin, G.P. and Shi, P.F., 2006. Effects of ozone treatment of carbon support on Pt–Ru/C catalysts performance for direct methanol fuel cell. *Carbon*, 44(1), pp.133-140.
29. Yu, X. and Ye, S., 2007. Recent advances in activity and durability enhancement of Pt/C catalytic cathode in PEMFC: Part I. Physico-chemical and electronic interaction between Pt and carbon support, and activity enhancement of Pt/C catalyst. *Journal of Power Sources*, 172(1), pp.133-144.

## 2. Chapter Two: Literature Review

### Chapter overview

This chapter reviews the current state of the art and history of fuel cells and its different types, focusing on proton exchange membrane fuel cells (PEMFCs). Their components and principles are described, emphasising in the cathode. In fact, since the focus of this thesis is the study of catalysts for the cathode of PEMFCs, the oxygen reduction reaction (ORR) on Pt, as well as its features and drawbacks are discussed. The use of Pt-Pd nanoparticles supported on carbon materials as cathode catalysts is also commented, highlighting the qualities that make them as suitable materials to perform the ORR.

### 2.1 Background



A fuel cell is a device that produces electricity from chemical reactions. As long as the fuel is supplied, the cell can continue producing electricity [1, 2]. Fuel cells are compatible with other renewable and modern energy sources, such as wind energy, solar energy and hydroelectricity, all of them devoted to a sustainable electricity production. Some of the characteristics associated to these devices are its silent operation without vibration, inherent modularity allowing to a simple construction and a diverse range of applications in portable devices, stationary units and transportation [3]. They provide a cleaner and more flexible chemical-to-electrical energy conversion than that offered by fossil fuel combustion. In this sense, it is important to highlight that combustion of fossil fuels has increased air pollution and the emission of greenhouse gasses such as CO<sub>2</sub>, leading to climate change, ozone depletion and acid rain [2, 4]. For these reasons, there has been intensive research and development of renewable and environmental friendly ways to generate electricity, since the Kyoto Protocol also suggested the use of renewable energy sources, the promotion of existing

high efficiency electricity technologies and the adoption of advanced low-CO<sub>2</sub> emission energy systems [2, 5].

The first fuel cell was presented by Sir William Grove in the early 1800s, who built a device that combines hydrogen and oxygen to produce electricity, being named as gas battery. Later, this device was known as fuel cell. In 1959, Francis Thomas Bacon presented the first fully-operational fuel cell [3, 4]. Nowadays, there are several types of fuel cells which have different chemical fuel feeds and operating principles.

## 2.2 Types of fuel cells

The fuels, operation temperatures and electrolytes used in the different types of fuel cells determine the operating conditions. Therefore, the most common fuel cells are:

### 2.2.1 Alkaline fuel cells (AFCs)

Alkaline fuel cells work with compressed hydrogen and oxygen, using a potassium hydroxide solution (KOH) in water as electrolyte. Its efficiency is close to 70 %, operating between 150 and 200 °C and yielding cell output ranges from 300 W to 5 kW. Some of the disadvantages of these devices are related with the use of pure hydrogen as fuel, the high cost of platinum as electrode catalyst and the liquid electrolyte leaking [5, 6-7].

### 2.2.2 Molten Carbonate fuel cells (MCFCs)

Molten carbonate fuel cells use molten sodium or magnesium carbonates as electrolytes. Efficiency ranges are between 60 to 80 %, operating at 650 °C. Some works reported performances up to 2 MW for a single stack and up to 100 MW for multi-stacks. In these cells, it is possible to limit the damage caused by carbon monoxide and recycle the heat produced during its operation. The low cost of these devices comes from the use of nickel

electro-catalysts, in comparison with the platinum electrodes used in other fuel cells. However, high operation temperatures limit the safety of MCFCs, as well as demand the use of corrosion-resistant materials [5, 6, 8].

### 2.2.3 Phosphoric acid fuel cells (PAFCs)

In these devices, phosphoric acid is used as electrolyte. Efficiency ranges are between 40 and 80 %, operating at 150 - 200 °C. Some phosphoric acid mono cells have shown outputs up to 200 kW, whereas the stacks have achieved 11 MW. PAFCs are more tolerant to carbon monoxide poisoning, broadening the range of possible substances able to be employed as fuels. However, the presence of phosphoric acid implies the design of highly corrosion-resistant parts for its building [5, 9].

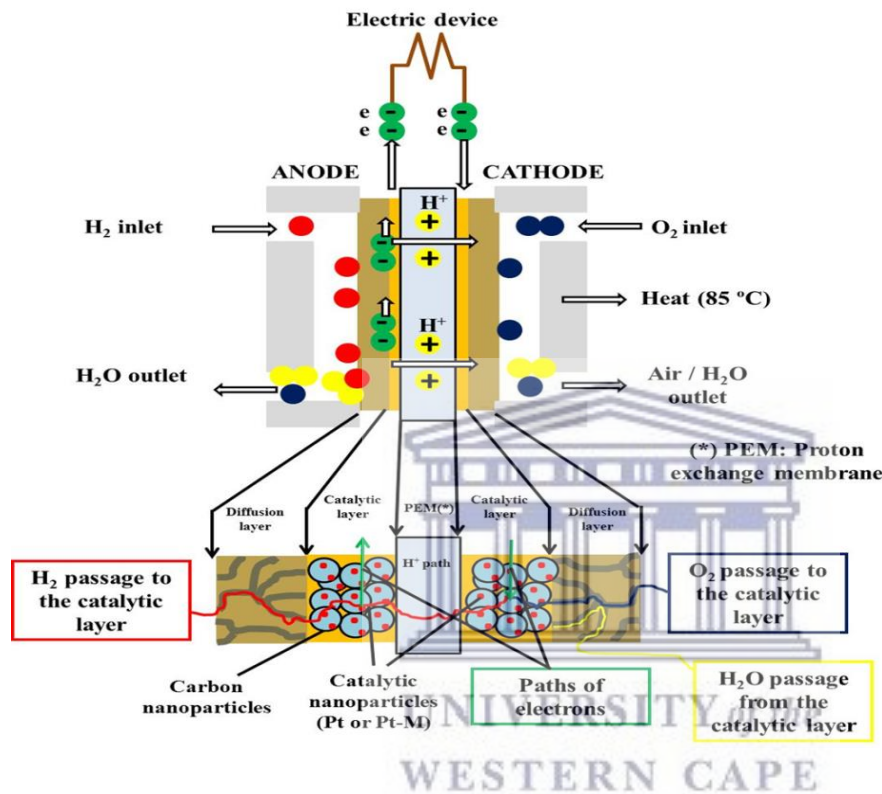
### 2.2.4 Solid Oxide fuel cells (SOFCs)

Solid oxide fuel cells use ceramic calcium or zirconium compounds as electrolytes. Efficiencies are close to 60 %, with working temperatures up to 1000 °C and outputs near to 100 kW. At these high temperatures, a reformer is not required to extract hydrogen from the fuel, although this factor also avoids the implementation of SOFCs in different electrical devices [5, 6, 10]

### 2.2.5 Proton exchange membrane fuel cell (PEMFCs)

The PEMFC uses a water-based acidic polymer membrane as electrolyte and platinum-based electrodes. PEMFCs were the first fuel cells to be used by the NASA in the 1960s [3]. Considerable improvements in this type of fuel cell were made from the early 1970s. Although they have been known over a long time, only in the early 1990s century they have become a subject of research bearing in mind the necessity for finding cleaner ways to

produce energy [4]. Their many advantages such as low operating temperatures (below 120°C), low weight, sustained operation at a high current density, easy start-ups, control of power outputs and compactness have promoted the attention of many researchers [5, 11].



Scheme 2.1: Scheme of a PEMFC (components and involved reactions) [12].

PEMFCs consist of an anode and a cathode separated by a membrane that allows the flow of the ions through it. The running of the cell starts when hydrogen is fed on the anode, which is usually obtained by water splitting or reforming of organic compounds such as natural gas, methanol or other liquid fuel [13, 14]. However, a lot of research needs to be performed about safer and cleaner ways to produce hydrogen, since the traditional methods result in the emission of pollutants such as carbon dioxide and carbon monoxide [11]. The oxidation of hydrogen can take place by two different pathways [15, 16]: (1) the chemical dissociation (1) or the electrochemical adsorption (2) of hydrogen on the catalyst





With M as a catalytic metal adsorbing and decomposing the H-H bond. Then, the adsorbed monoatomic hydrogen is oxidised (3):



Once the electrons are produced, they go through the electrical circuit, while protons cross through the proton exchange membrane to reach the cathode (see Figure 1) [6, 17]. The union between the membrane and the two catalytic layers constitute the membrane electrode assembly (MEA). This catalytic layer is generally conformed by platinum, which is a common element in both the anode and the cathode. Once the protons reach the cathode, they react with oxygen, which is fed on the cathode. The mechanism for the oxygen reduction reaction is detailed described in the section 2.4, which global process is described by the equation:



Thus, the global reaction in the PEMFC is represented by:



### 2.3 High temperature PEMFCs

Low temperatures PEMFCs (LT-PEMFCs) suffer several limitations, related with the low operating temperature, the complex water management to prevent the flooding inside the MEA and the adsorption of poisonous species such as carbon monoxide (CO) on the anode, which come with the hydrogen produced by the hydrocarbons reformat process [18, 19] and



competes with hydrogen for the adsorption on the Pt active sites. Nevertheless, at temperatures around 130 °C platinum-based catalysts can tolerate up to 1000 ppm CO, while at 80 °C the platinum catalysts can tolerate only 10 ppm [20].

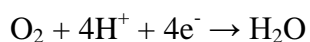
The increase in the temperature means a decrease in the resistance of the exchange membranes. For this reason, in the last years, polymer membranes have been developed for operation at temperatures up to 230°C. When these membranes are employed, the PEMFCs are known as high temperature PEMFCs (HT-PEMFCs). Since HT-PEMFCs have a higher CO tolerance, they can work with low-purity hydrogen, avoiding the gas humidification while the high temperature can be used on other processes such as cogeneration of heat and power or on-board reforming [21- 24]. This fact offers a significant advantage as many stages of fuel processing can be removed thus allowing for cost-effective fuel. Moreover, less CO in the cell means a high availability of active sites for hydrogen adsorption on platinum and thus overall improvement in the performance of the cell.

Regarding the oxygen reduction reaction (ORR) occurring on the fuel cell cathode, its slow kinetic affects the performance of the PEMFCs. As a consequence, an overpotential is required to perform this reaction, which results in cell voltage losses. A partial solution to this drawback is the increase in the operation temperatures, which enhances the ORR kinetics [25]. On the other hand, the presence of platinum in the cathode contributes significantly to the high cost of the PEMFC; therefore, the use of a low cost material for the cathodes can contribute to the reducing of the fuel cell cost. This fact led to a lot of research about alternative catalysts for the PEMFC cathode. The use of platinum group metals [26] and alloys between Pt and other non-noble metals supported on carbon structures [27] has been reported to have similar performances compared with those for the traditional platinum catalysts.

## 2.4 Oxygen reduction reaction

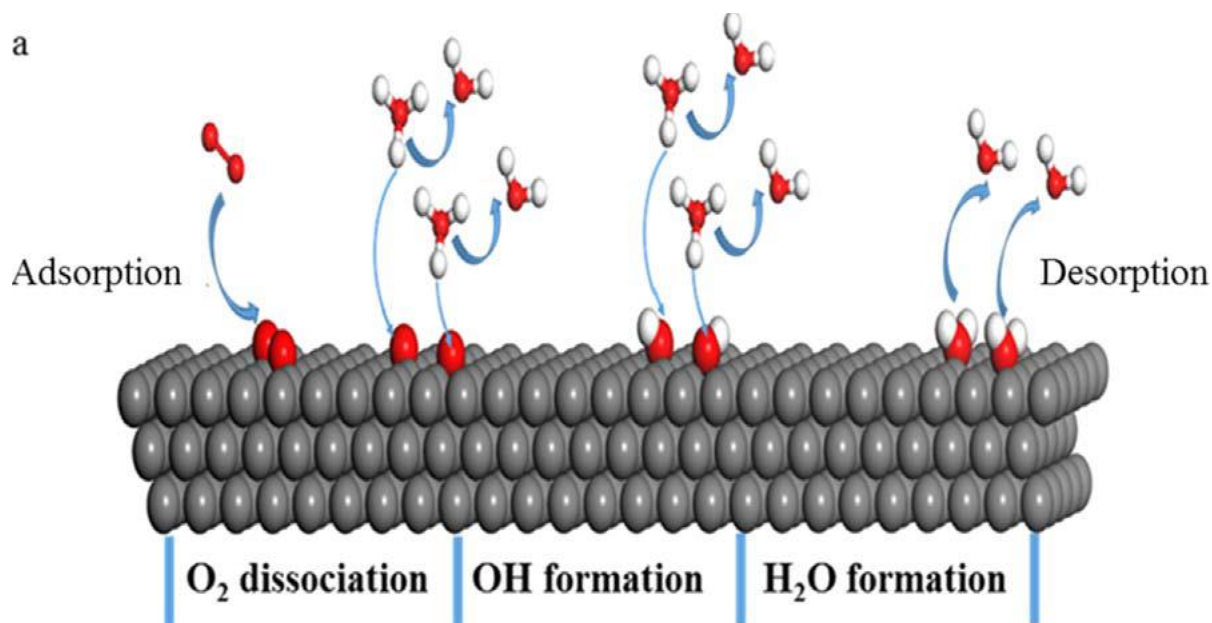
A wide research has been focussed in the mechanism of the ORR when it is performed on Pt, since this reaction is sensitive to the properties of the surface and the presence of other adsorbed species on the catalyst. In order to increase the performance of the ORR, the mechanism and kinetics of the oxygen reduction reaction have been studied on a great variety of electrode materials and electrolytes. These studies concluded that a high over potential is required to carry out the ORR observed in low temperature fuel cells [4].

The ORR occurs in two pathways and results in the production of water and the involvement of four electrons [28, 29]. However, because of the characteristics of the mechanism, it is also possible to produce hydrogen peroxide, which involves only two electrons during the reaction. It means a decrease in the performance of the cathode, besides the corrosion of some parts of the fuel cell, bearing in mind the high oxidising capacity of H<sub>2</sub>O<sub>2</sub> [30]. The reduction of oxygen involving four electrons and producing water is described by:



UNIVERSITY of the  
WESTERN CAPE

(6)



*Scheme 2.2: Schematic representation of the total reduction of oxygen [31]*

However, when the oxygen reduction is not completed, the formation of hydrogen peroxide takes place, involving only two electrons:

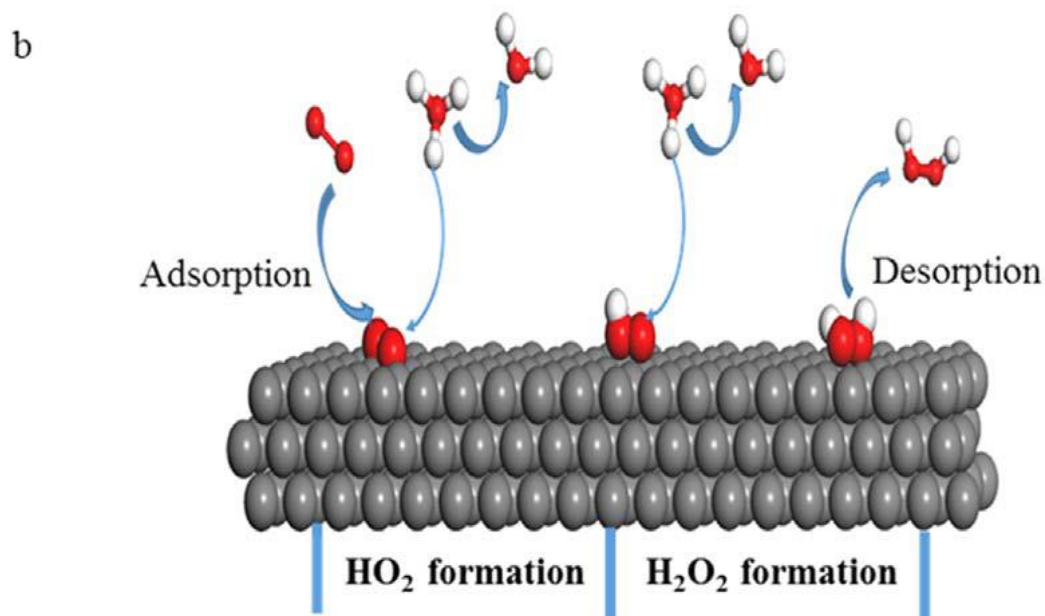


This  $\text{H}_2\text{O}_2$  can be reduced to water, following the reaction:



According with the Figure 2, the ORR starts with the adsorption of oxygen on the surface of two adjacent platinum atoms. Once the water is formed, this is desorbed from the catalyst surface.

Nevertheless, in some cases the dissociation of molecular oxygen does not occur after its adsorption. Therefore, the hydrogenation stages occur incompletely, as shown in Figure 3, generating hydrogen peroxide and involving only two electrons in the reaction [31].



*Scheme 2.3: Schematic representation of the partial reduction of oxygen [31].*

## 2.5 Platinum catalysts

Platinum is traditionally used as a catalyst in the cathode of the PEMFCs, usually in the form of nanoparticles supported on a carbon material, due to some advantages such as: (1) stability against corrosive environments caused by the low pH high temperatures and potential fluctuations. This factor avoids the use of transition metals in their pure forms [32]; (2) high activity toward the ORR, facilitating both the adsorption and dissociation of molecular oxygen [33]; (3) it must release the products from the surface once the reaction is complete, addressing the reaction toward the formation of desired products [34]. It is important to highlight that in the case of the ORR, the water formation pathway involves four electrons, meaning the highest performance for this reaction, while the hydrogen peroxide formation pathway only involves two electrons, besides its corrosive potential to the cell [35]. Therefore, the catalyst must optimise the production of water [36]. (4) It must be able to be resistant to poisoning by impurities coming from the feed gases.

## 2.6 Platinum alloys

Using Pt alloys with other elements is an alternative to improve the activity of the catalysts [37]. It includes binary, ternary and quaternary Pt alloys, Pt-based metal oxide catalysts [38], Pt-based composites and organic metal complexes [39] and carbon-supported transition-metal porphyrin catalysts [40]. In the case of the cathode, Pt is usually alloyed with metals such as Co, Pd, Cu and Ni, providing stability against the dissolution of the less noble metal. On the other hand, the electronic structure of Pt is modified by the presence of the second metal, improving the ORR activity [41].

One of the metals alloyed with Pt to perform the ORR is palladium, which is able to induce a change in the electronic structure of Pt that increases its activity toward the ORR [42]. Peng and Yang prepared carbon supported platinum-on-palladium (Pt/Pd/C) bimetallic heterogeneous nanostructure, in which 3-nm Pt nanoparticles grew on the surface of 5 nm-Pd nanoparticles. The electrochemical study showed an enhancement in the electrocatalytic activity for ORR with improved stability in comparison to a commercial platinum catalyst [43]. Other studies have demonstrated that Pd enters into the face-centered cubic structure of Pt, reducing the distance between two platinum atoms and therefore, promoting the adsorption of oxygen atoms on the catalytic surface [44].

## 2.7 Carbon Supports

Carbon materials have been used as supports for catalysts of the PEMFC to improve the stability and activity of the catalytic nanoparticles [45]. To achieve this purpose, the carbon material must fulfil have a high electrical conductivity to allow the electronic transference, large surface area to disperse properly the nanoparticles, outstanding corrosion resistance, strong interaction with the nanoparticle, and a pore size that enables the diffusion of the

electroactive species [46]. Thus, the selection of a carbon support with adequate properties is a crucial decision to influence properly the durability and activity of the catalyst [47]. There are different carbon supports commonly employed in the PEMFC electrodes, including carbon blacks [48], carbon nanofibers [49], carbon nanotubes [50], carbon xerogels [51] and graphenes [52].

### 2.7.1 Carbon Blacks

Carbon blacks have been used as catalytic support since the 1990s. These materials are produced by oil and acetylene furnace combustion processes. Their large surface area, high electrical conductivity, well-developed pore structure, high availability and low cost have attracted the attention of researchers [53]. However, the main disadvantage of carbon blacks is its highly rich microporous structure which inhibits the diffusion of the electroactive species.

### 2.7.2 Carbon nanofibers

Carbon nanofibers are produced by the thermal decomposition of hydrocarbons over NiAlCu catalysts [54]. They have several structures depending on their graphitic plane organisation such as *ribbon*, *platelet* and *herringbone* [55]. When carbon nanofibers are used as support for electrode catalysts in PEMFCs, its high length to diameter ratio allows the formation of conducting networks in the Nafion<sup>®</sup> membrane matrix, a fact that contributes to the improved performance of the catalysts [56].

### 2.7.3 Carbon nanotubes

Carbon nanotubes (CNTs) are the most well-known carbon nanostructures for application as catalyst support in fuel cells [57]. They are 2-dimensional nanostructural tubes typically

formed by rolled up-single sheets of hexagonally arranged carbon atoms. The carbon nanotubes can be single walled (SWCNTs: single-walled carbon nanotubes) or multi-walled (MWCNTs: multi-walled carbon nanotubes). SWCNTs can be either conducting or semi conducting depending on their chiral vector nature, while MWCNTs have higher conductivity than SWCNTs [45]. The inert character of these structures can be modified by functionalisation of their surface using strong acids. In fact, the functionalisation process promotes a better dispersion of the nanoparticles, better particle size control and dispersion and also tuned morphologies [58].

#### 2.7.4 Carbon xerogels

Carbon xerogels (CX) are characterised by its high surface area, high content of mesopores, low micro porosity and high corrosion resistance [59]. Particularly, the large porous size of CX increases the diffusion of electro-active species toward the catalytic nanoparticles. In fact, the pore texture can easily be tailored from diameters in the range of nanometres to micrometers [60]. Moreover, the surface chemistry tuning permits the design of supports with improved abilities to disperse the Pt on its surface, enhanced mass transport in the operating conditions and a strong Pt-Nafion contact [61].



## References

1. O'hayre, R., Cha, S.W., Prinz, F.B. and Colella, W., 2016. *Fuel cell fundamentals*. John Wiley & Sons.
2. Elmer, T., Worall, M., Wu, S. and Riffat, S.B., 2015. Fuel cell technology for domestic built environment applications: State of-the-art review. *Renewable and Sustainable Energy Reviews*, 42, pp.913-931.
3. Sharaf, O.Z. and Orhan, M.F., 2014. An overview of fuel cell technology: Fundamentals and applications. *Renewable and Sustainable Energy Reviews*, 32, pp.810-853.
4. Fernandez Alvarez, G., 2011. Palladium based catalysts for oxygen reduction in polymer electrolyte membrane fuel cells (Doctoral thesis, Newcastle University). [accessed online, 28 February 2017]
5. Lucia, U., 2014. Overview on fuel cells. *Renewable and Sustainable Energy Reviews*, 30, pp.164-169.
6. Steele, B.C. and Heinzel, A., 2011. Materials for fuel-cell technologies. In *Materials For Sustainable Energy: A Collection of Peer-Reviewed Research and Review Articles from Nature Publishing Group* (pp. 224-231).
7. Coutanceau, C., Demarconnay, L., Lamy, C. and Léger, J.M., 2006. Development of electrocatalysts for solid alkaline fuel cell (SAFC). *Journal of Power Sources*, 156(1), pp.14-19.
8. Dicks, A.L., 2004. Molten carbonate fuel cells. *Current Opinion in Solid State and Materials Science*, 8(5), pp.379-383.



9. Johnson Matthey 2018, FuelCellToday, accessed 22 March 2018, <http://www.fuelcelltoday.com/technologies/pemfc>
10. Singhal, S.C., 2007. Solid oxide fuel cells. *The Electrochemical Society Interface*, 16(4), p.41.
11. Wee, J.H., 2007. Applications of proton exchange membrane fuel cell systems. *Renewable and sustainable energy reviews*, 11(8), pp.1720-1738.
12. Şengül, E., Erkan, S., Eroğlu, İ. and Bac, N., 2008. Effect of gas diffusion layer characteristics and addition of pore-forming agents on the performance of polymer electrolyte membrane fuel cells. *Chemical Engineering Communications*, 196(1-2), pp.161-170.
13. Mehta, V. and Cooper, J.S., 2003. Review and analysis of PEM fuel cell design and manufacturing. *Journal of Power Sources*, 114(1), pp.32-53.
14. Wu, J., Yuan, X.Z., Martin, J.J., Wang, H., Zhang, J., Shen, J., Wu, S. and Merida, W., 2008. A review of PEM fuel cell durability: Degradation mechanisms and mitigation strategies. *Journal of Power Sources*, 184(1), pp.104-119.
15. Mello, R.M. and Ticianelli, E.A., 1997. Kinetic study of the hydrogen oxidation reaction on platinum and Nafion® covered platinum electrodes. *Electrochimica Acta*, 42(6), pp.1031-1039.
16. Shao, M., 2011. Palladium-based electrocatalysts for hydrogen oxidation and oxygen reduction reactions. *Journal of Power Sources*, 196(5), pp.2433-2444.

17. Wang, Y., Chen, K.S., Mishler, J., Cho, S.C. and Adroher, X.C., 2011. A review of polymer electrolyte membrane fuel cells: technology, applications, and needs on fundamental research. *Applied energy*, 88(4), pp.981-1007.
18. Li, Q., He, R., Gao, J.A., Jensen, J.O. and Bjerrum, N.J., 2003. The CO poisoning effect in PEMFCs operational at temperatures up to 200 C. *Journal of the Electrochemical Society*, 150(12), pp.A1599-A1605.
19. Haque, M.A., Sulong, A.B., Loh, K.S., Majlan, E.H., Husaini, T. and Rosli, R.E., 2017. Acid doped polybenzimidazoles based membrane electrode assembly for high temperature proton exchange membrane fuel cell: A review. *International Journal of Hydrogen Energy*, 42(14), pp.9156-9179.
20. Gang, X., Qingfeng, L., Hjuler, H.A. and Bjerrum, N.J., 1995. Hydrogen oxidation on gas diffusion electrodes for phosphoric acid fuel cells in the presence of carbon monoxide and oxygen. *Journal of the Electrochemical Society*, 142(9), pp.2890-2893.
21. Liu, Y., Lehnert, W., Janßen, H., Samsun, R.C. and Stolten, D., 2016. A review of high-temperature polymer electrolyte membrane fuel-cell (HT-PEMFC)-based auxiliary power units for diesel-powered road vehicles. *Journal of Power Sources*, 311, pp.91-102.
22. Gervasio, D., 2007, September. High Temperature Polymer Electrolyte Membrane Fuel Cell (HT PEMFC) Portable Power Source. In *Meeting Abstracts* (No. 3, pp. 195-195). The Electrochemical Society.

23. Zhang, W., Li, M.K.S., Yue, P.L. and Gao, P., 2008. Exfoliated Pt-clay/Nafion nanocomposite membrane for self-humidifying polymer electrolyte fuel cells. *Langmuir*, 24(6), pp.2663-2670.
24. Asensio, J.A., Sánchez, E.M. and Gómez-Romero, P., 2010. Proton-conducting membranes based on benzimidazole polymers for high-temperature PEM fuel cells. A chemical quest. *Chemical Society Reviews*, 39(8), pp.3210-3239.
25. Chandan, A., Hattenberger, M., El-Kharouf, A., Du, S., Dhir, A., Self, V., Pollet, B.G., Ingram, A. and Bujalski, W., 2013. High temperature (HT) polymer electrolyte membrane fuel cells (PEMFC)–A review. *Journal of Power Sources*, 231, pp.264-278.
26. Pollet, B.G., Pasupathi, S., Swart, G., Mouton, K., Lototsky, M., Williams, M., Bujlo, P., Ji, S., Bladergroen, B.J. and Linkov, V., 2014. Hydrogen South Africa (HySA) systems competence centre: mission, objectives, technological achievements and breakthroughs. *International journal of hydrogen energy*, 39(8), pp.3577-3596.
27. Wang, Y.J., Fang, B., Li, H., Bi, X.T. and Wang, H., 2016. Progress in modified carbon support materials for Pt and Pt-alloy cathode catalysts in polymer electrolyte membrane fuel cells. *Progress in Materials Science*, 82, pp.445-498.
28. Lim, D.H. and Wilcox, J., 2012. Mechanisms of the oxygen reduction reaction on defective graphene-supported Pt nanoparticles from first-principles. *The Journal of Physical Chemistry C*, 116(5), pp.3653-3660.

29. Zhang, L. and Xia, Z., 2011. Mechanisms of oxygen reduction reaction on nitrogen-doped graphene for fuel cells. *The Journal of Physical Chemistry C*, 115(22), pp.11170-11176.
30. Holton, O.T. and Stevenson, J.W., 2013. The role of platinum in proton exchange membrane fuel cells. *Platinum Metals Review*, 57(4), pp.259-271.
31. Stacy, J., Regmi, Y.N., Leonard, B. and Fan, M., 2017. The recent progress and future of oxygen reduction reaction catalysis: A review. *Renewable and Sustainable Energy Reviews*, 69, pp.401-414.
32. Paulus, U.A., Schmidt, T.J., Gasteiger, H.A. and Behm, R.J., 2001. Oxygen reduction on a high-surface area Pt/Vulcan carbon catalyst: a thin-film rotating ring-disk electrode study. *Journal of Electroanalytical Chemistry*, 495(2), pp.134-145.
33. Antolini, E., Salgado, J.R. and Gonzalez, E.R., 2006. The stability of Pt–M (M= first row transition metal) alloy catalysts and its effect on the activity in low temperature fuel cells: a literature review and tests on a Pt–Co catalyst. *Journal of Power Sources*, 160(2), pp.957-968.
34. Borup, R., Meyers, J., Pivovar, B., Kim, Y.S., Mukundan, R., Garland, N., Myers, D., Wilson, M., Garzon, F., Wood, D. and Zelenay, P., 2007. Scientific aspects of polymer electrolyte fuel cell durability and degradation. *Chemical reviews*, 107(10), pp.3904-3951.
35. Shao-Horn, Y., Sheng, W.C., Chen, S., Ferreira, P.J., Holby, E.F. and Morgan, D., 2007. Instability of supported platinum nanoparticles in low-temperature fuel cells. *Topics in Catalysis*, 46(3-4), pp.285-305.

36. Yaowarat, W., 2016. Enhancement of durability by silica coating Pt-based catalysts for fuel cell application.
37. Wang, H., Xu, C., Cheng, F., Zhang, M., Wang, S. and Jiang, S.P., 2008. Pd/Pt core-shell nanowire arrays as highly effective electrocatalysts for methanol electrooxidation in direct methanol fuel cells. *Electrochemistry Communications*, 10(10), pp.1575-1578.
38. Pereira, L.G.S., dos Santos, F.R., Pereira, M.E., Paganin, V.A. and Ticianelli, E.A., 2006. CO tolerance effects of tungsten-based PEMFC anodes. *Electrochimica acta*, 51(19), pp.4061-4066.
39. Yano, H., Ono, C., Shiroishi, H. and Okada, T., 2005. New CO tolerant electrocatalysts exceeding Pt-Ru for the anode of fuel cells. *Chemical Communications*, (9), pp.1212-1214.
40. Antolini, E., Salgado, J.R. and Gonzalez, E.R., 2006. The stability of Pt-M (M= first row transition metal) alloy catalysts and its effect on the activity in low temperature fuel cells: a literature review and tests on a Pt-Co catalyst. *Journal of Power Sources*, 160(2), pp.957-968.
41. Stamenkovic, V., Mun, B.S., Mayrhofer, K.J., Ross, P.N., Markovic, N.M., Rossmeisl, J., Greeley, J. and Nørskov, J.K., 2006. Changing the activity of electrocatalysts for oxygen reduction by tuning the surface electronic structure. *Angewandte Chemie*, 118(18), pp.2963-2967.
42. Shao, M., Liu, P., Zhang, J. and Adzic, R., 2007. Origin of enhanced activity in palladium alloy electrocatalysts for oxygen reduction reaction. *The Journal of Physical Chemistry B*, 111(24), pp.6772-6775.

43. Peng, Z. and Yang, H., 2009. Synthesis and oxygen reduction electrocatalytic property of Pt-on-Pd bimetallic heteronanostructures. *Journal of the American Chemical Society*, 131(22), pp.7542-7543.
44. Calderón, J.C., Ndzuzo, L., Bladergroen, B.J. and Pasupathi, S., 2018. Catalytic activity of carbon supported-Pt-Pd nanoparticles toward the oxygen reduction reaction. *Materials Today: Proceedings*, 5(4), pp.10551-10560.
45. Sharma, S. and Pollet, B.G., 2012. Support materials for PEMFC and DMFC electrocatalysts—a review. *Journal of Power Sources*, 208, pp.96-119.
46. Jha, N., Reddy, A.L.M., Shaijumon, M.M., Rajalakshmi, N. and Ramaprabhu, S., 2008. Pt–Ru/multi-walled carbon nanotubes as electrocatalysts for direct methanol fuel cell. *International Journal of Hydrogen Energy*, 33(1), pp.427-433.
47. Yu, X. and Ye, S., 2007. Recent advances in activity and durability enhancement of Pt/C catalytic cathode in PEMFC: Part I. Physico-chemical and electronic interaction between Pt and carbon support, and activity enhancement of Pt/C catalyst. *Journal of Power Sources*, 172(1), pp.133-144.
48. Wang, J., Yin, G., Shao, Y., Zhang, S., Wang, Z. and Gao, Y., 2007. Effect of carbon black support corrosion on the durability of Pt/C catalyst. *Journal of Power sources*, 171(2), pp.331-339.
49. Wang, Y., Jin, J., Yang, S., Li, G. and Qiao, J., 2015. Highly active and stable platinum catalyst supported on porous carbon nanofibers for improved performance of PEMFC. *Electrochimica Acta*, 177, pp.181-189.

50. Wang, X., Li, W., Chen, Z., Waje, M. and Yan, Y., 2006. Durability investigation of carbon nanotube as catalyst support for proton exchange membrane fuel cell. *Journal of Power Sources*, 158(1), pp.154-159.
51. Figueiredo, J.L. and Pereira, M.F., 2013. Synthesis and functionalization of carbon xerogels to be used as supports for fuel cell catalysts. *Journal of Energy Chemistry*, 22(2), pp.195-201.
52. Stambula, S., Gauquelin, N., Bugnet, M., Gorantla, S., Turner, S., Sun, S., Liu, J., Zhang, G., Sun, X. and Botton, G.A., 2014. Chemical structure of nitrogen-doped graphene with single platinum atoms and atomic clusters as a platform for the PEMFC electrode. *The Journal of Physical Chemistry C*, 118(8), pp.3890-3900.
53. Antolini, E., 2009. Carbon supports for low-temperature fuel cell catalysts. *Applied Catalysis B: Environmental*, 88(1-2), pp.1-24.
54. Rodriguez, N.M., Kim, M.S. and Baker, R.T.K., 1994. Carbon nanofibers: a unique catalyst support medium. *The journal of physical chemistry*, 98(50), pp.13108-13111.
55. Zheng, J.S., Zhang, X.S., Li, P., Zhu, J., Zhou, X.G. and Yuan, W.K., 2007. Effect of carbon nanofiber microstructure on oxygen reduction activity of supported palladium electrocatalyst. *Electrochemistry Communications*, 9(5), pp.895-900.
56. Li, W., Waje, M., Chen, Z., Larsen, P. and Yan, Y., 2010. Platinum nanoparticles supported on stacked-cup carbon nanofibers as electrocatalysts for proton exchange membrane fuel cell. *Carbon*, 48(4), pp.995-1003.
57. Dudin, P.V., Unwin, P.R. and Macpherson, J.V., 2010. Electrochemical nucleation and growth of gold nanoparticles on single-walled carbon nanotubes: New



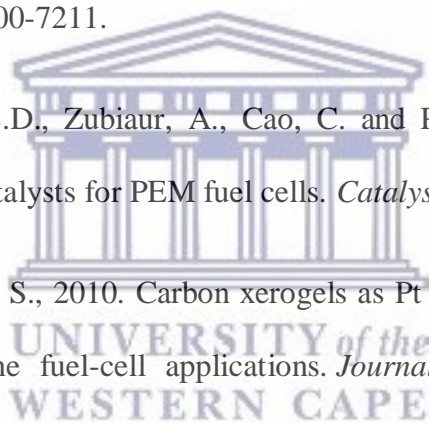
mechanistic insights. *The Journal of Physical Chemistry C*, 114(31), pp.13241-13248.

58. Wang, C.H., Du, H.Y., Tsai, Y.T., Chen, C.P., Huang, C.J., Chen, L.C., Chen, K.H. and Shih, H.C., 2007. High performance of low electrocatalysts loading on CNT directly grown on carbon cloth for DMFC. *Journal of Power Sources*, 171(1), pp.55-62.

59. Calderón, J.C., Mahata, N., Pereira, M.F.R., Figueiredo, J.L., Fernandes, V.R., Rangel, C.M., Calvillo, L., Lázaro, M.J. and Pastor, E., 2012. Pt–Ru catalysts supported on carbon xerogels for PEM fuel cells. *international journal of hydrogen energy*, 37(8), pp.7200-7211.

60. Job, N., Lambert, S.D., Zubiaur, A., Cao, C. and Pirard, J.P., 2015. Design of Pt/carbon xerogel catalysts for PEM fuel cells. *Catalysts*, 5(1), pp.40-57.

61. Liu, B. and Creager, S., 2010. Carbon xerogels as Pt catalyst supports for polymer electrolyte membrane fuel-cell applications. *Journal of Power Sources*, 195(7), pp.1812-1820.





## 3. Chapter Three: Materials and methods

### Overview

This chapter reports the different chemicals used during this study, as well as the detailed description of the experimental procedures followed to prepare the catalysts. Moreover, a description of the physical and electrochemical characterisation techniques used to study the physical and electrochemical properties of the as-synthesised materials is presented.

### 3.1 Experimental

#### 3.1.1 Chemicals

The chemicals used in this study include: chloroplatinic acid solution ( $\text{H}_2\text{PtCl}_6$ , 8%, w/w, Sigma-Aldrich), potassium tetrachloropalladate II ( $\text{K}_2\text{PdCl}_4$ , 98%, Sigma-Aldrich), ethanol (94-96%, Sigma Aldrich), Nafion<sup>®</sup> (5%, dispersed in low weight alcohols, Sigma-Aldrich), carbon black, carbon nanofibers, carbon xerogels (Nanolit), *n*-propanol ( $\text{C}_3\text{H}_8\text{O}$ , 99.7%, Sigma-Aldrich), sodium carbonate ( $\text{Na}_2\text{CO}_3$ , 99.5%, Sigma-Aldrich), methanol ( $\text{CH}_3\text{O}$ , 99.8%, anhydrous, Sigma-Aldrich), formaldehyde ( $\text{CH}_2\text{O}$ , 37w.% in  $\text{H}_2\text{O}$ , Sigma-Aldrich), N-dodecyl-N,N-dimethyl-3-ammonio-1-propanesulfonate ( $\text{C}_{17}\text{H}_{39}\text{NO}_3\text{S}$ , 98%, Sigma-Aldrich), sodium hydroxide ( $\text{NaOH}$ , 98%, anhydrous, Sigma-Aldrich), L-ascorbic acid ( $\text{C}_6\text{H}_8\text{O}_6$ , Sigma-Adrich), perchloric acid ( $\text{HClO}_4$ , ACS reagent, 70%, Sigma-Aldrich), hydrogen (99.990%  $\text{H}_2$ , Air Liquide<sup>®</sup>), nitrogen (90.999%  $\text{N}_2$ , Air Liquide<sup>®</sup>), hydrochloric acid ( $\text{HCl}$ , 32%, KMIX).

## 3.1.2 Synthesis of carbon-supported Pt-Pd nanoparticles

### 3.1.2.1 Synthesis using Ethanol as a reducing agent

In this method, 30 mg of the carbon support were mixed with 0.5  $\mu\text{L}$  of Nafion<sup>®</sup>, 20 mL of ethanol and 30 mL of milli-Q water (Millipak<sup>®</sup> Express 40). The mixture was dispersed in the ultrasonic bath for 30 minutes. Afterwards, the chloroplatinic acid and potassium tetrachloropalladate (II) solution prepared in 8 mL of ethanol and 12 mL of water was dropped to the carbon dispersion in presence of ultrasound. Once the addition of the metal precursors was finished, the reaction mixture was kept in the ultrasound bath for 30 minutes. Then, the mixture was refluxed at 82 °C during 3 hours. Once the mixture was cooled down, the pH of the mixture was adjusted to 8.5 and stirred for 48 hours. The resulting Pt-Pd/C-EtOH catalyst was then filtered, washed with ultrapure water and dried at 80 °C. In the name of the catalyst, C could be CB as carbon black, CNF as carbon nanofibers and CX as carbon xerogels. The same procedure was performed replacing the ethanol by *n*-propanol as solvent, generating the catalyst Pt-Pd/C-*n*PrOH.

### 3.1.2.2 Synthesis using Formaldehyde as a reducing agent

30 mg of carbon support was mixed with 40 mL of water and 140 mg of sodium carbonate. The dispersion was stirred in the ultrasonic bath for 30 minutes at room temperature. Then, a 20 mL-solution containing the metal precursors were slowly added to the mixture at 80° C. Afterwards, 100 $\mu\text{l}$  of formaldehyde were added and keep stirring for 3 hours at 80° C[1]. The mixture was kept in the stirrer for 48 hours and then filtered, washed and dried at 80°C. The as-obtained catalyst was heat-treated under a hydrogen/nitrogen reductant atmosphere for 2 hours at 300°C to finally obtain a catalyst labelled as Pt-Pt/C-FMY.

### 3.1.2.3 Synthesis using Methanol as the reducing agent

In this procedure, 30 mg of carbon support were added to 40 mL of methanol, 120 mL of water and 12,5 mg of N-Dodecyl-N,N-dimethyl-3-ammonio-1-propanesulfonate [2]. The mixture was stirred in the ultrasonic sound bath for 30 minutes and then under reflux until the temperature of the mixture reached 90°C. Afterwards, the solution of the metal precursors in 10 mL of methanol and 30 mL of water was dropped into the dispersion. Once the addition of the metal precursors was finished, the reaction mixture was kept under reflux for one hour at 90 °C. The dispersion was allowed to cool down at room temperature in stirring for 48 hours. Finally, the mixture was filtered, washed and dried in the oven at 80°C overnight. The as-prepared catalyst has been labelled with the name Pt-Pd/C-MeOH.

### 3.1.2.4 Synthesis using ascorbic acid as reducing agent.

30 mg of carbon support were dispersed in 50 mL of water. The dispersion was put in the ultrasound bath for 30 minutes. The metal precursors were dissolved in 40 mL of water and this solution was dropwise added into the carbon dispersion. The mixture was stirred in the ultrasound bath for 30 minutes. Subsequently, 500 mg of ascorbic acid were added and the reaction mixture was stirred in the ultrasound bath for 30 minutes. Afterwards, the mixture was refluxed for 6 hours at 85 °C, followed by cooling down at room temperature for 48 hours. The solution was then filtered, washed and dried in the oven overnight at 80 °C [3]. The as-prepared catalyst has been labelled with the name Pt-Pd/C-AA.

### 3.1.3 Characterisation techniques

#### 3.1.3.1 Physical characterisation

The metal content and Pt:Pd atomic ratios of the as-synthesised catalysts were determined by energy-dispersive X-ray (EDX) analysis, employing a scanning electron microscope (Zeiss-Auriga) working at 20 keV, with a Si detector and a Be window. X ray diffraction (XRD) patterns were obtained by means of a D8 Advance diffractometer (Bruker AXS), operating with a Cu-K $\alpha$  radiation generated at 40 kV and 40 mA. The dispersion and particle size distribution of the catalytic nanoparticles were studied by transmission electron microscopy (TEM), using a transmission electron microscope (200 kV FEI Tecnai G2 20) coupled to a CCD Gatan camera, which generated the images. These images were treated with the ImageJ<sup>®</sup> software. Textural properties of carbon supports and catalysts were calculated from nitrogen adsorption–desorption isotherms, measured at -196 °C using a Micromeritics ASAP 2020. Microporosity was determined from *t*-plot method.

#### 3.1.3.2 Electrochemical characterisation

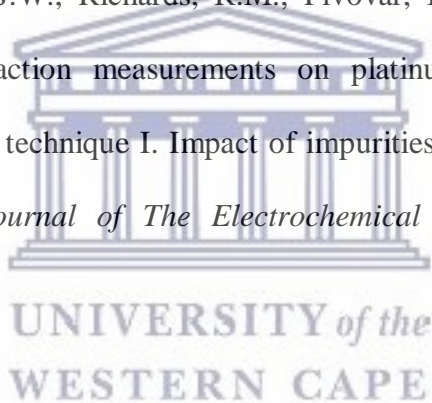
A three-electrode cell at 25 °C coupled to an Autolab<sup>®</sup> PGSTAT302N potentiostat-galvanostat was used to perform the electrochemical characterisation of the catalysts. A Pt mesh acted as counter electrode, while the reference electrode was a Ag/AgCl electrode (3 M KCl, Metrohm<sup>®</sup>). A rotating disk electrode (RDE, Pine Research Instrumentation) with a glassy carbon disk (geometric area = 0.196 cm<sup>2</sup>) was used to support the synthesized catalysts. An aliquot of a catalyst ink (20  $\mu$ L) was dried onto the glassy carbon disk at rotating speed of 700 rpm, in order to employ it as working electrode. The ink was prepared by ultrasound-mixing of 2 mg of catalyst with 10.5  $\mu$ L of Nafion<sup>®</sup>, 630  $\mu$ L of isopropyl alcohol and 2 mL of ultrapure water [4].

$N_2$  was employed to deoxygenate all solutions. The activation of the working electrode was performed between 0.05 and 1.0 V at  $20 \text{ mV s}^{-1}$ , making 75 cycles in the  $O_2$ -free supporting electrolyte. Afterwards, 3 cycles between -0.020 and 1.0 V *vs* RHE at  $20 \text{ mV s}^{-1}$  were recorded. CO-stripping measurements were made in order to determine the activity of the catalysts toward the poisoning of this adsorbate. CO was bubbled into the electrochemical cell for 10 min at 0.2 V *vs* RHE, in order to form a monolayer on the deposited catalyst. After, nitrogen was bubbled for 20 min to remove the CO from the electrolyte and five potential scans at  $20 \text{ mV s}^{-1}$ , between -0.020 and 1.0 V *vs* RHE were applied. The area under the CO oxidation peak was employed to calculate the electroactive area, assuming a charge of  $420 \mu\text{C cm}^{-2}$  involved in the oxidation of a linearly adsorbed CO monolayer. The currents obtained by cyclic voltammetry and presented in this thesis have been normalised by this electroactive area. For the ORR experiments,  $O_2$  was bubbled 30 min at 1.0 V before each experiment, maintaining a soft bubbling during all measurements. Steady-state polarization curves at  $2 \text{ mV s}^{-1}$  were recorded between 1.0 and 0 V with 200, 400, 600, 900, 1200, 1600, 2000 and 2500 rpm as rotating speeds, to evaluate the catalysts activity toward the ORR.

Durability tests of the catalysts were performed, performing 2000 cycles between 0.05 and 1.0 V *vs* RHE, at  $50 \text{ mV s}^{-1}$  in the  $O_2$ -free support electrolyte. Before and after the cycling process, the support electrolyte was bubbled with  $O_2$  during 30 min and steady-state polarization curves at 1600 rpm were recorded. All the currents corresponding to the ORR experiments presented in this thesis have been normalised by the geometric area.

## References

1. Zhang, L., Lee, K. and Zhang, J., 2007. Effect of synthetic reducing agents on morphology and ORR activity of carbon-supported nano-Pd–Co alloy electrocatalysts. *Electrochimica Acta*, 52(28), pp.7964-7971.
2. Wang, X. and Hsing, I.M., 2002. Surfactant stabilized Pt and Pt alloy electrocatalyst for polymer electrolyte fuel cells. *Electrochimica acta*, 47(18), pp.2981-2987.
3. Zhang, Y., Chang, G., Shu, H., Oyama, M., Liu, X. and He, Y., 2014. Synthesis of Pt–Pd bimetallic nanoparticles anchored on graphene for highly active methanol electro-oxidation. *Journal of Power Sources*, 262, pp.279-285.
4. Shinozaki, K., Zack, J.W., Richards, R.M., Pivovar, B.S. and Kocha, S.S., 2015. Oxygen reduction reaction measurements on platinum electrocatalysts utilizing rotating disk electrode technique I. Impact of impurities, measurement protocols and applied corrections. *Journal of The Electrochemical Society*, 162(10), pp.F1144-F1158.



## 4. Chapter Four: Results and Discussion

### Overview

This chapter presents and discusses the results obtained from the physical and electrochemical characterisation of the synthesised Pt-Pt catalysts supported on carbon xerogels (CX), carbon black (CB) and carbon nanofibers (CNF), which were reduced with methanol (MeOH), *n*-propanol (nPrOH), formaldehyde (FMY), ethanol (EtOH) and ascorbic acid (AA). The physical characterisation was performed by means of X-ray diffraction (XRD), energy-dispersive spectroscopy (EDS) and transmission electron microscopy (TEM), whereas the electrochemical characterisation was carried out by cyclic voltammetry (CV) and rotating disc electrode (RDE). These results have been compared with those reported in the literature and the obtained from a commercial available Pt /C Alfa Aesar catalyst.

### 4.1 Physical characterisation

#### 4.1.1 Composition and particle sizes of the synthesised catalysts

##### 4.1.1.1 Composition and particle sizes of Pt-Pd/CX

Table 4.1 summarises the results obtained from the physical characterisation of the synthesised Pt-Pd/CX catalysts. The aim of the study was to prepare catalysts with a metal content close to 40 wt. % and the EDS analysis showed values between 34-38 wt. %, while the metal content for the commercial Pt/C catalyst was around 34 wt. %. It is also remarkable the low Pt content in the synthesised catalysts (between 15.3 and 18 wt %), compared with that of the commercial one. The obtaining of low Pt content is an important fact in this study, since one of our goals was to reduce the content of Pt in these materials. All the catalysts demonstrated a Pt:Pd atomic ratio close to 1:2, as experimentally planned, suggesting that the



employed reducing agents are suitable for the synthesis of Pt-Pd nanoparticles with the planned nominal values. The lattice parameters were calculated using the equation 4.1:

$$a_{fcc} = \frac{\sqrt{h^2 + k^2 + l^2} \lambda_{K\alpha 1}}{\text{sen}\theta_{\max}} \quad 4.1$$

with  $h$ ,  $k$  and  $l$  as the Miller index,  $\lambda_{K\alpha 1}$  as the X-ray source wavelength,  $\theta_{\max}$  as the Bragg angle and  $a_{fcc}$  as the lattice parameter. This parameter was lower than that of Pt/C (3.916 Å), particularly in the case of Pt-Pd/CX-nPrOH, Pt-Pd/CX-FMY and Pt-Pd/CX-AA, indicating the formation of an alloy between platinum and palladium [1, 2].

Table 4.1. Physical characterisation of the synthesized Pt-Pd/CX catalysts

Catalyst	Atomic ratio Pt:Pd	Metal or Pt content/wt. %		Crystallite or particle size/nm		Lattice parameter/Å	Metal surface area/ m <sup>2</sup> g <sup>-1</sup>
		Metal	Pt	XRD	TEM		
Pt-Pd/CX-MeOH	30:70	38	15.4	7.4	4.3 ± 1.0	3.917	50
Pt-Pd/CX-EtOH	34:66	37	18.0	9.5	3.2 ± 0.6	3.918	38
Pt-Pd/CX-nPrOH	31:69	34	15.3	7.8	3.0 ± 0.7	3.899	47
Pt-Pd/CX-FMY	34:66	35	17.2	8.5	5.4 ± 2.5	3.908	43
Pt-Pd/CX-AA	35:65	36	18.0	12.8	4.3 ± 1.7	3.898	28
Pt/C Alfa Aesar	...	34	34	3.3	3.1 ± 1.4	3.916	85

#### 4.1.1.2 Composition and particle size of Pt-Pd/CB

Table 4.2 presents the results from the physical characterisation of the Pt-Pd/CB catalysts. The metal content of these materials was close to 40 wt. % and the Pt-Pd atomic ratio was near to 1:2, as planned. Similar to the case of the carbon xerogel-supported materials, a remarkable fact was the obtaining of low Pt contents between 14 wt. % and 19wt. %. In



general, the Pt-Pd/CB catalysts showed particle sizes similar and even lower than that of the commercial catalyst, except in the case of the catalyst reduced with formaldehyde. On the other hand, there was a reduction in the lattice parameter compared to that of Pt/C except in the case of Pt-Pd/CX-MeOH, confirming the formation of an alloy between platinum and palladium.

Table 4.2. Physical characterisation of the synthesized Pt-Pd/CB catalysts.

Catalyst	Atomic	Metal or Pt		Crystallite or		Lattice	Metal surface
	ratio	content/wt. %		particle size/ nm		Parameter/ Å	area/ m <sup>2</sup> .g <sup>-1</sup>
	Pt:Pd	Metal	Pt	XRD	TEM		
Pt-Pd/CB- MeOH	37:67	31	16	3.9	3.8 ± 2.1	3.917	90
Pt-Pd/CB-EtOH	30:70	31	14	3.6	2.9 ± 1.9	3.903	104
Pt-Pd/CB-nPrOH	33:67	40	19	4.9	3.3 ± 1.1	3.902	75
Pt-Pd/CB-FMY	35:65	39	19	3.8	6.0 ± 2.5	3.907	95
Pt-Pd/CB-AA	34:66	37	18	4.2	2.7 ± 1.5	3.903	85
Pt/C Alfa Aesar	...	34	34	3.3	3.1 ± 1.4	3.916	85

#### 4.1.1.3 Composition and particle size of Pt-Pd/CNF

The results obtained for the physical characterisation of the catalysts supported on carbon nanofibers are showed in Table 4.3. The atomic ratio values in the catalysts reduced with methanol, ethanol and ascorbic acid were close to 1:2, although the metal contents of the catalysts were below 40 wt. %, with Pt-Pd/CNF-nPrOH achieving the high metal content among this group of catalysts (31 wt. %). This result suggests that there was not a good interaction between carbon nanofibers and the metal precursors in these synthesis routes. On the other hand, the obtaining of lattice parameters lower than that of the commercial catalyst

demonstrated the formation of a Pt-Pd alloy. The crystallite size was employed to calculate the metal surface area, by means of the equation:

$$SA \text{ (m}^2 \text{ g}^{-1}\text{)} = 6000/d\rho_{Pt-Pd} \quad 4.2$$

Where  $d$  is the crystallite size (nm) and  $\rho_{Pt-Pd}$  is the alloy density.  $\rho_{Pt-Pd}$  was calculated by means of the expression  $\rho_{Pt-Pd} \text{ (g cm}^{-3}\text{)} = \rho_{Pt}X_{Pt} + \rho_{Pd}X_{Pd}$ , where  $\rho_{Pt}$  is the platinum density (21.4 g cm<sup>-3</sup>),  $\rho_{Pd}$  is the palladium density (12.0 g cm<sup>-3</sup>), and  $X_{Pt}$  and  $X_{Pd}$  are the weight percentage of Pt and Pd, respectively. The biggest surface area was recorded with the catalysts reduced with methanol (94 m<sup>2</sup> g<sup>-1</sup>), overcoming that one of Pt/C (85 m<sup>2</sup> g<sup>-1</sup>). All the catalysts supported on carbon black, except in the case of the material reduced with *n*-propanol displayed bigger surface areas than that of Pt/C. This can be attributed to the large surface area of carbon black, which allows dispersion of metal nanoparticles [3]. On the other hand, the catalysts supported on carbon xerogels displayed lower surface areas compared to the commercial Pt/C catalyst, which means a minor number of active sites on the metal nanoparticles surface.

Table 4.3. Physical characterisation of the synthesised Pt-Pd/CNF catalysts

Catalyst	Atomic	Metal/Pt		Crystallite or		Lattice	Metal surface area/m <sup>2</sup> g <sup>-1</sup>
	ratio	content/wt. %		particle size/nm		parameter/Å	
	Pt:Pd	Metal	Pt	XRD	TEM		
Pt-Pd/CNF-MeOH	33:67	23	11	3.9	4.7 ± 1.5	3.919	94
Pt-Pd/CNF-EtOH	33:67	23	11	5.3	2.9 ± 1.1	3.903	70
Pt-Pd/CNF-nPrOH	43:57	31	19	5.0	2.7 ± 1.5	3.909	69
Pt-Pd/CNF-FMY	43:57	28	17	4.6	5.5 ± 1.5	3.903	77
Pt-Pd/CNF-AA	34:66	14	9	5.4	2.6 ± 0.7	3.891	63
Pt/C Alfa Aesar	...	34	34	3.3	3.1 ± 1.4	3.916	85

### 4.1.1 X-Ray diffraction (XRD) characterisation of the synthesised catalysts

The XRD patterns for the catalysts supported on carbon xerogels are depicted in Figure 4.1. The typical (111), (200), (220), (311) and (222) peaks of the Pt face-centred cubic (fcc) structure were observed at 40, 47, 67, 82, and 89° 2θ, respectively. These reflections showed a shift toward high 2θ values, respect to the peaks observed for the commercial Pt/C catalyst, as a consequence of the entrance of Pd into the Pt structure, forming an alloy [4]. In the case of the catalyst Pt-Pd/CX-EtOH, the shift was not evident, matching the low variation in its lattice parameter (see Table 4.1) and suggesting that in this material, there are Pt and Pd nanoparticles deposited on the carbon xerogels besides Pt-Pd alloyed nanoparticles. Regarding the crystallite sizes, they were calculated using the dimensions of the (220) peak and the Debye-Scherrer equation [5]:

$$D = \frac{K\lambda}{\beta \cos\theta} \quad 4.3$$

Where  $K$  is the Scherrer constant,  $D$  is the average particle size,  $\theta$  is the diffraction angle,  $\beta$  is the width and  $\lambda$  is the X-ray wavelength. These values are summarised in the Table 4.1. The crystallite sizes of the carbon xerogel-supported catalysts were larger than 7 nm, whereas the particle sizes detected by TEM were lower than 5.5 nm, indicating that the synthesis routes promote the formation of amorphous particles with short diameter. The crystallite size is larger than the particle size due to the employed measurement method; In XRD, an average of all the crystalline particles is obtained, even those which are aggregated, since the X ray beam crosses all the crystallites in the material. As a consequence, the X ray beam considers the agglomerated crystallites as only one particle, increasing the crystallite size value. In TEM, only the well-defined nanoparticles are considered to measure the diameter and the agglomerated nanoparticles are disregarded. The lowest crystallite size was determined for

the catalyst reduced with methanol (Pt-Pd/CX-MeOH, 7.4 nm) whereas the largest one was found for the catalyst prepared in presence of ascorbic acid (Pt-Pd/CX-AA, 12.8 nm).

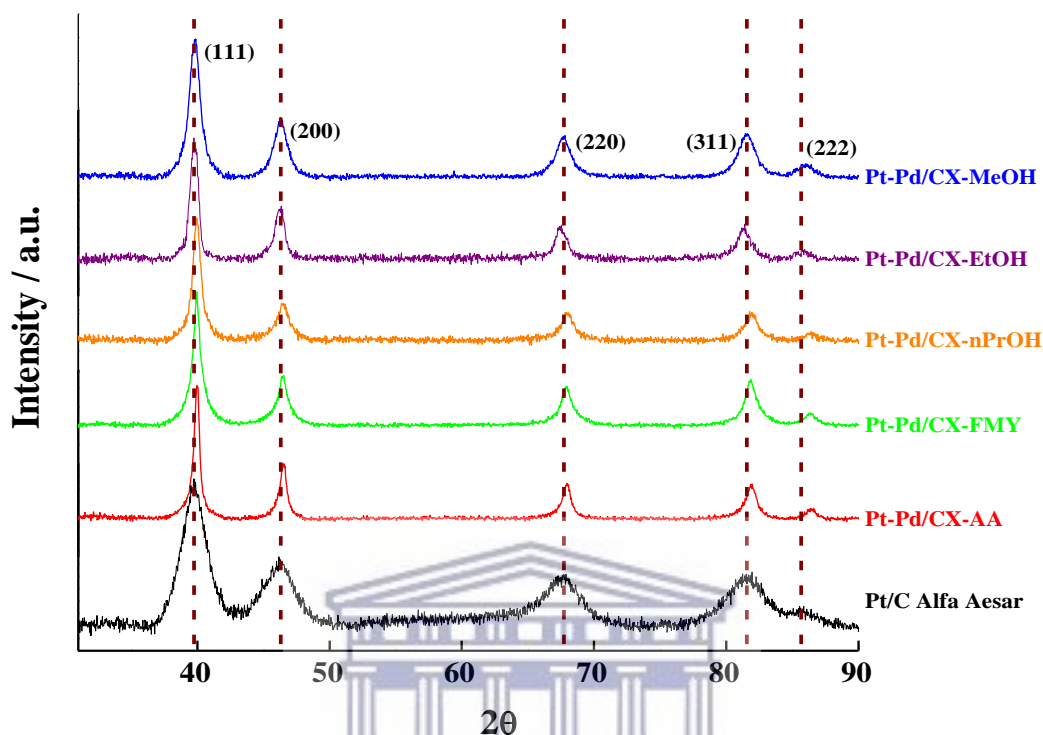


Figure 4.1 XRD patterns of synthesised Pt-Pd/CX and the commercial Pt/C catalysts.

The XRD patterns of the Pt-Pd/CB catalysts are presented in Figure 4.2. A low intensity peak around  $25^\circ$  was observed, which corresponds to the reflection of the (002) graphitic planes of carbon black. A slight shift in the reflections of Pt-Pd respect to those of the commercial Pt/C was detected, confirming the entrance of Pd into the Pt fcc structure. On the other hand, the crystallite size was determined and values from 4.9 nm to 3.6 nm were calculated, with Pt-Pd/CB-nPrOH exhibiting the biggest value and Pt-Pd/CB-EtOH the lowest one. On the other hand, the highest lattice parameter was found for Pt-Pd/CB-MeOH indicating there is a low alloying degree between Pt and Pd when methanol is used as a reducing agent, being this result similar to that observed for the catalysts supported on carbon xerogels. The other catalysts displayed a smaller lattice parameter value and an evident shift in the XRD patterns, confirming the high alloying degree between Pt and Pd.

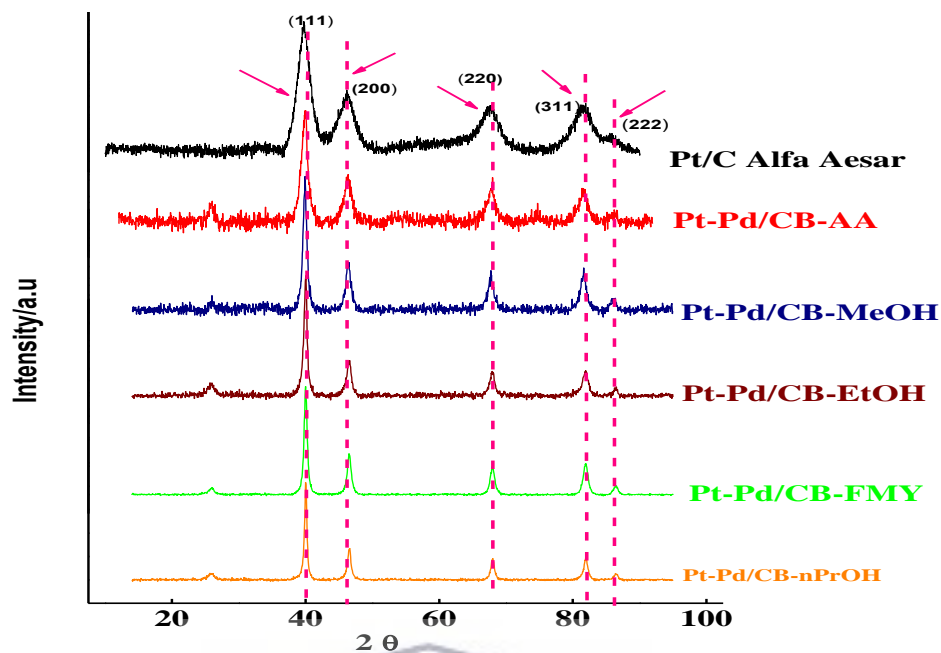


Figure 4.2 XRD patterns of synthesised Pt-Pd/CB and the commercial Pt/C catalysts.

Figure 4.3 shows the XRD patterns of the catalysts supported on carbon nanofibers. For these materials, the peak corresponding to the (002) graphitic planes developed a higher intensity, due to the high content of these planes in this carbon material [5]. Similar to the other studied materials, the reflections were shifted toward higher  $2\theta$  degrees. Regarding the crystallite sizes, the largest value was determined for Pt-Pd/CNF-AA (5.4 nm) and the smallest for Pt-Pd/CNF-MeOH (3.9 nm). Among these materials, the highest lattice parameter was obtained for the catalyst reduced with methanol, meaning a low alloying degree between Pt and Pd when this reducing agent is employed.

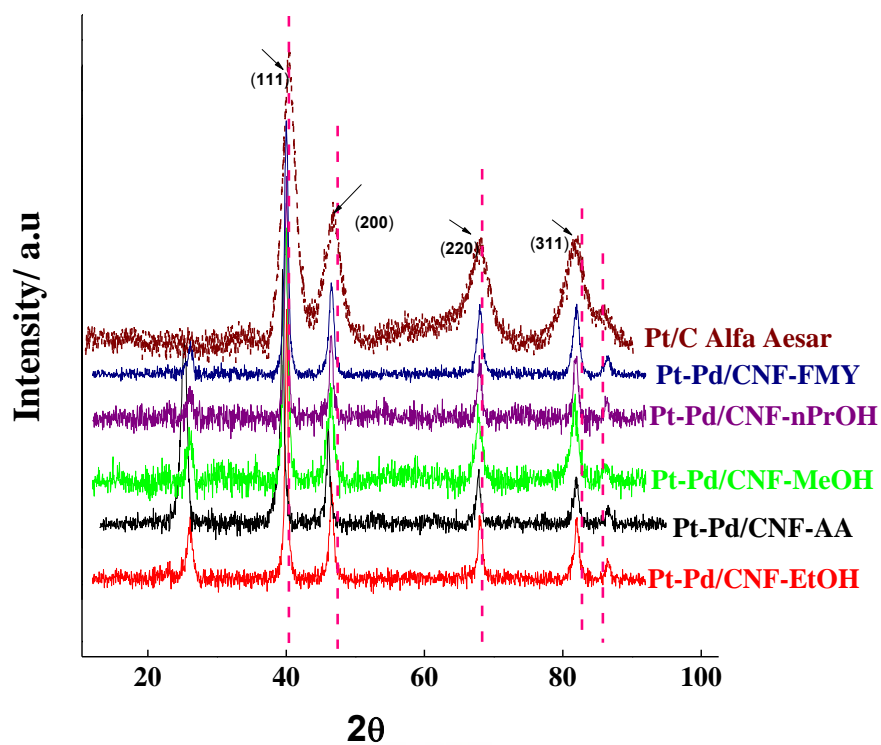


Figure 4.3 XRD patterns of synthesised Pt-Pd/CNF and the commercial Pt/C catalysts.

#### 4.1.2 Transmission electron microscopy (TEM) characterisation of the synthesised catalysts

Figure 4.4 shows the micrographs obtained from the TEM analysis of the Pt-Pd/CX catalysts. The metal nanoparticles demonstrated a high dispersion on the carbon xerogels, a fact explained from the encapsulation effect of the organic molecules and surfactants employed during the synthesis procedures, which inhibit the agglomeration between the nanoparticles. The catalyst synthesised with *n*-propanol as reducing agent exhibited the narrowest distribution in terms of the diameters, followed by the catalysts prepared in presence of ethanol and methanol, indicating that the longest carbon chain of the alcohols promotes the formation of nanoparticles with the smallest diameters. This fact was observed in previous works focussed in the synthesis of Pt-alloyed nanoparticles in presence of long carbon chain alcohols [6]. On the other hand, the agglomerated nanoparticles as well as the wide particle size dispersion of the catalyst reduced with formaldehyde indicate a low encapsulating



capacity of this molecule. It is important to consider that water was the main solvent in the catalysts reduced with formaldehyde and ascorbic acid, suggesting that presence of water as main solvent in the mentioned synthesis routes increases the particle size distribution. Therefore, these results verified the role of primary alcohols as reducing agents and encapsulating molecules to address the obtaining of well-dispersed nanoparticles with narrow size distributions [7-9].

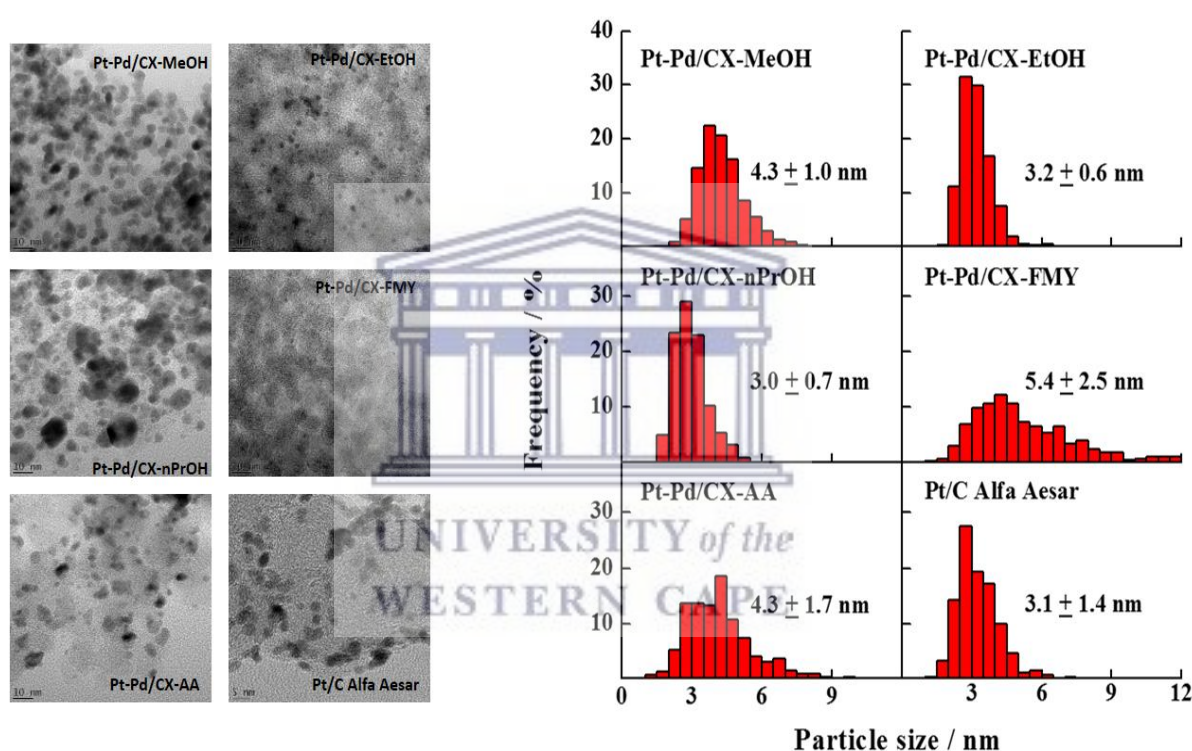


Figure 4.4 TEM images and histograms of Pt-Pd/CX and the commercial Pt/C catalysts.

The TEM photographs of the catalysts supported on carbon black are shown in Figure 4.5. In general, these materials showed good dispersion of nanoparticles on carbon black although those reduced with *n*-propanol, methanol and formaldehyde showed a wide size distribution, while the catalysts reduced with ethanol and ascorbic acid showed a narrow distribution.

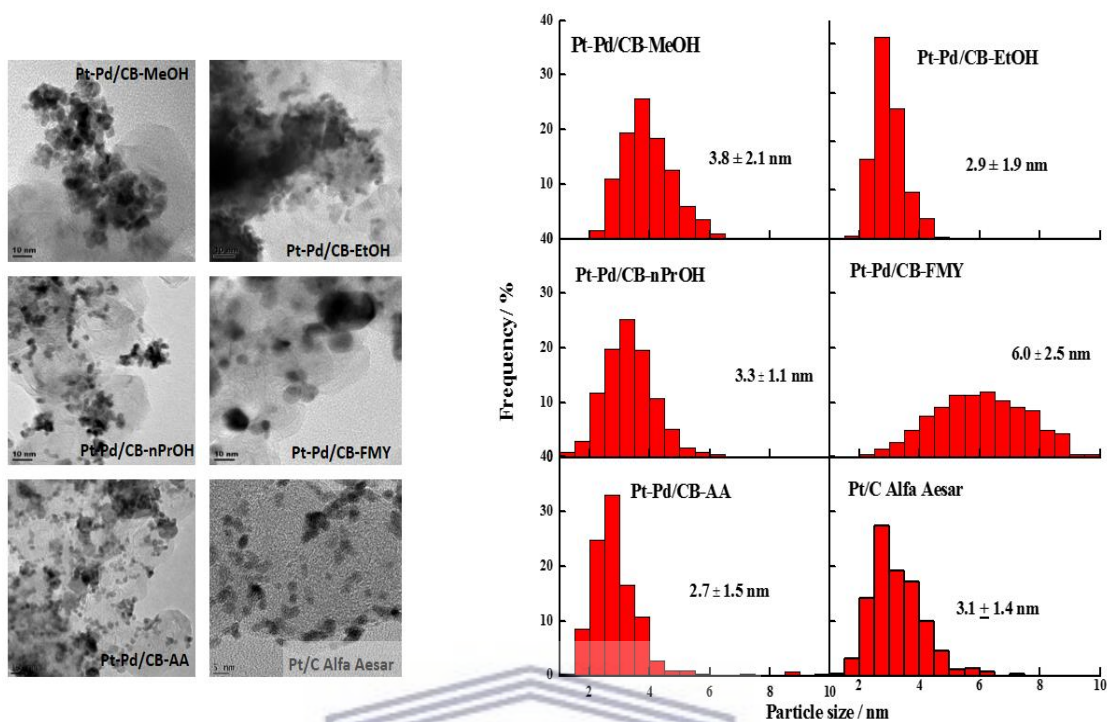


Figure 4.5 TEM images and histograms of Pt-Pd/CB and the commercial Pt/C catalysts.

In the case of the catalysts supported on carbon nanofibers (Pt-Pd/CNF), a very good dispersion of the nanoparticles on the carbon support was observed (see Figure 4.6). Again, the catalysts reduced with methanol and formaldehyde showed a wide particle size distribution while the materials reduced with ethanol, *n*-propanol and ascorbic acid showed a narrower distribution of nanoparticles, suggesting that on carbon nanofibers, the use of small molecules as reducing agent promotes the formation of nanoparticles with short diameter.



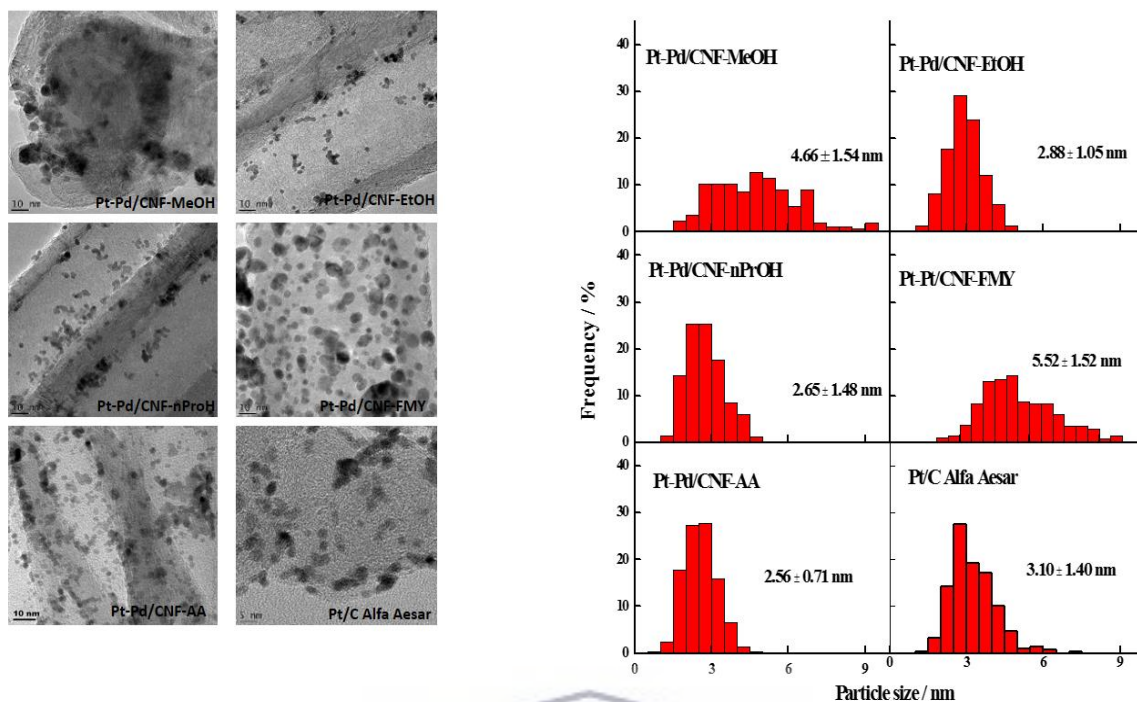


Figure 4.6 TEM images and histograms of Pt-Pd/CB and the commercial Pt/C catalysts.

## 4.2 Electrochemical characterisation

### 4.2.1 Cyclic voltammetry

Figure 4.7 depicts the electrochemical characterisation of the synthesised carbon xerogel-supported catalysts in the electrolyte. For these experiments, the currents have been normalised by the electrochemical surface areas (ECSA), which were determined from the CO stripping as described in the section 3.1.3.2 and reported in Table 4.4. The cyclic voltammograms show the typical signals for the hydrogen adsorption/desorption process in the range of -0.010 to 0.3 V vs RHE, the capacitive currents between 0.3 V and 0.6 V and the formation of Pt oxides at high potentials at 0.6 - 1.0 V with its respective reduction peak around 0.730 V. The catalysts synthesised with ethanol and *n*-propanol developed higher current densities for hydrogen evolution compared with the materials reduced with ascorbic acid, methanol and formaldehyde. Nevertheless, a poor definition of the peaks corresponding

to the hydrogen desorption process, compared to those of the commercial Pt/C catalyst was observed. This fact can be attributed to the presence of palladium that adsorbs and also absorbs hydrogen. On the other hand, the potential values for the reduction of the metal oxides formed during the forward scan were more positive for all the Pt-Pd/CX than that of Pt/C. The presence of Pd might facilitate the reduction of these oxides and enables the formation of more active sites to increase the catalytic activity.

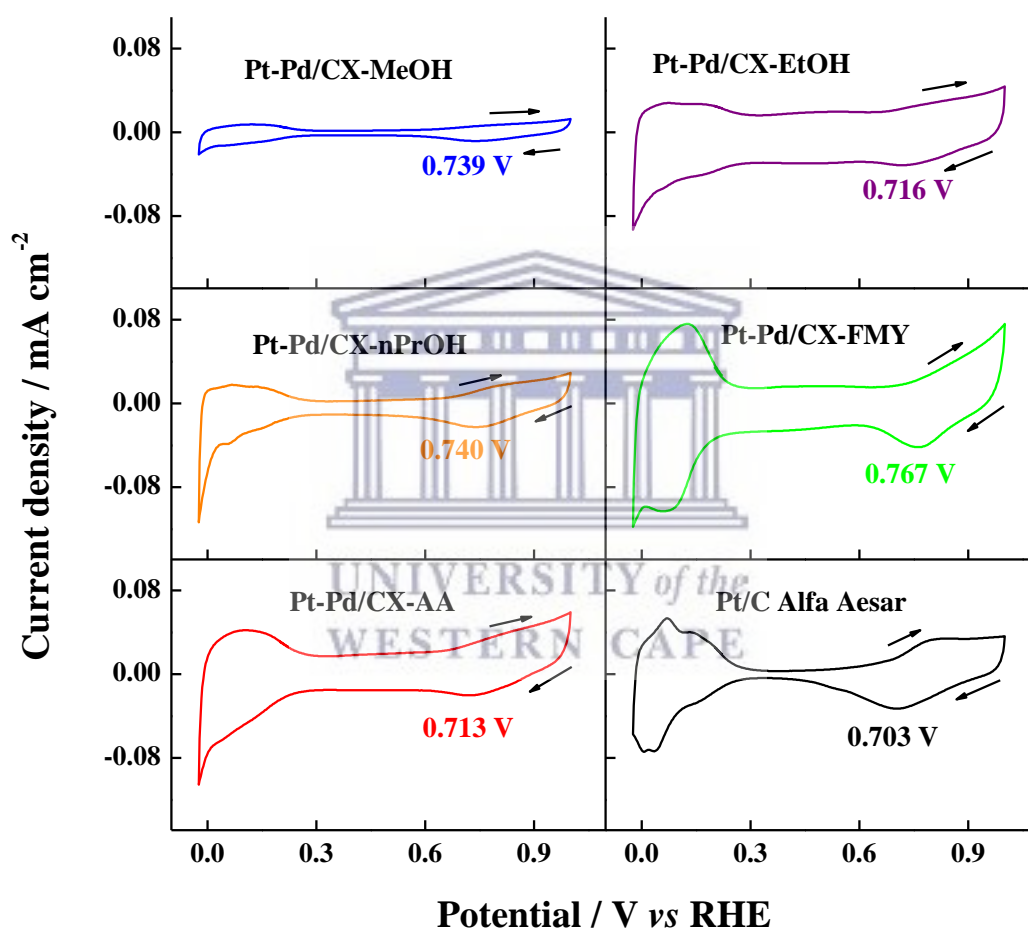


Figure 4.7 Cyclic voltammograms of the Pt-Pd/CX and the commercial Pt/C catalysts in the supporting electrolyte (0.1 M HClO<sub>4</sub>). Scan rate: 20 mV s<sup>-1</sup>.

In the case of the materials supported on carbon black, the electrochemical signals were the same observed for the catalysts supported on carbon xerogels. The catalysts reduced with methanol and ascorbic acid displayed higher current densities for the evolution of hydrogen

compared to the materials reduced with ethanol, *n*-propanol and formaldehyde. In comparison with the catalysts supported on carbon xerogels, the potential values for the reduction of the Pt oxides in the carbon black-supported catalysts were more positive. This fact indicates that the presence of graphitic planes in this carbon material increases the activity of the Pt-Pd nanoparticles, bearing in mind that these graphitic planes were not detected by XRD in the Pt-Pd/CX catalysts.

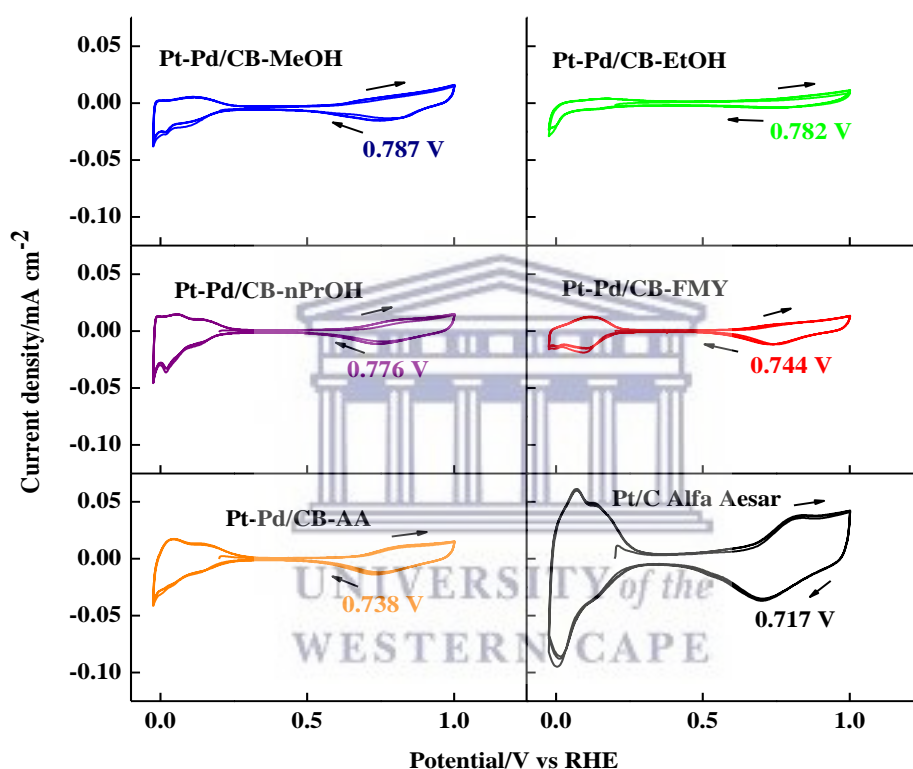


Figure 4.8 Cyclic voltammograms of the Pt-Pd/CB and the commercial Pt/C catalysts in the supporting electrolyte (0.1 M HClO<sub>4</sub>). Scan rate: 20 mV s<sup>-1</sup>.

Figure 4.9 presents the cyclic voltammograms of the synthesised catalysts supported on carbon nanofibers. Similar to the catalysts previously described, the typical signals for the hydrogen adsorption and desorption process were in the range between 0.010 and 0.3 V vs RHE. The catalyst developing the highest current densities for the evolution of hydrogen was

Pt-Pd/CNF-EtOH. Regarding the catalyst Pt-Pd/CNF-MeOH, this material developed the most positive potential corresponding to the reduction of metal oxides among all the studied catalysts.

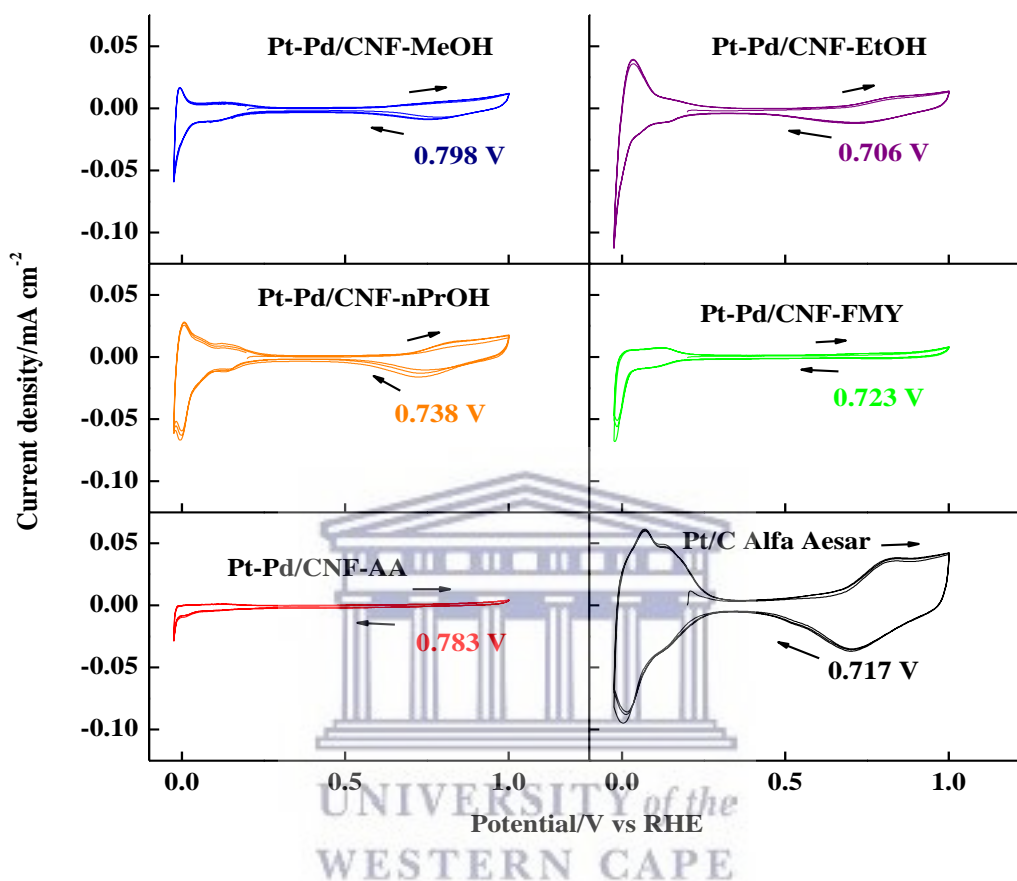


Figure 4.9 Cyclic voltammograms of the Pt-Pd/CNF and the commercial Pt/C catalysts in the supporting electrolyte (0.1 M HClO<sub>4</sub>). Scan rate: 20 mV s<sup>-1</sup>.

The electrochemical surface area (ECSA) of the synthesised Pt-Pd and the commercial Pt/C catalysts are reported in Table 4.4. The ECSA of a catalyst affects the reaction rate, the activity inside a fuel cell and the obtained current/power densities [10]. Pt-Pd/CX-MeOH, Pt-Pd/CX-AA and Pt-Pt/CB-AA were the only materials displayed ECSA values higher than that of the commercial catalyst.

Table 4.4. Electrochemical surface area (ECSA) of the studied catalysts.

Catalysts	ECSA / m <sup>2</sup> g <sub>Pt</sub> <sup>-1</sup>		
	CX	CB	CNF
Pt-Pd-MeOH	154.72	61.81	46.02
Pt-Pd-EtOH	38.83	70.91	94.65
Pt-Pd-nPrOH	52.36	54.42	46.47
Pt-Pd-FMY	62.02	56.39	45.35
Pt-Pd-AA	115.81	113.84	94.28
Pt/C Alfa Aesar	...	98.0	...

#### 4.2.2 Activity towards ORR

The activity of the studied carbon xerogel-supported catalysts toward the oxygen reduction reaction performed at 2500, 2000, 1600, 1200, 900, 600, 400 and 200 rpm was assessed and the results are presented in the Figure 4.10. The synthesised catalysts Pt-Pd/CX-MeOH, Pt-Pd/CX-EtOH and Pt-Pd/CX-FMY exhibited the more positive onset potential at 2500 rpm (0.883 V and 0.792 V, respectively, see Table 4.5) compared to those of the other catalysts. This result indicates that a lower activation energy is required to start the electrochemical reduction of oxygen on the mentioned catalysts. On the other hand, the materials Pt-Pd/CX-nPrOH, and Pt-Pd/CX-AA displayed similar onset potentials, which were 0.760 and 0.756 V, respectively. However, this sequence, changed on the half-wave potential since the catalysts reduced with formaldehyde and methanol developed the more positive values compared to the other materials. In this case, Pt/C generated the most positive half-wave potential at 0.717 V, which means it requires the lowest energy to kinetically control the ORR at 2500 rpm. Pt-Pd/CX-FMY and Pt-Pd/CX-MeOH displayed the highest diffusional current densities among

the synthesised catalysts followed by Pt-Pd/CX-nPrOH, Pt-Pd/CX-EtOH and Pt-Pd/CX-AA. Pt/C exhibited a higher diffusional current density compared to the Pt-Pd/CX materials. Nevertheless, the obtaining of high diffusional currents demonstrates that Pd plays an important role in the activity of the synthesised catalysts [11], promoting a synergy effect on Pt that induces the obtaining of higher current outputs. It is well-known that the presence of Pd induces a decrease in the Pt-Pt interatomic distance, which enables the oxygen adsorption and thus, the activity of the catalysts. Due this fact, the obtaining of higher outputs for these materials during the PEM fuel cell operation when they are used as cathodes could be expected. Another remarkable fact was related with the activity of Pt-Pd/CX-MeOH, which exhibited the smallest crystallite size and also developed high diffusional current densities, which indicates that the availability of active sites to carry out ORR is inversely proportional to the crystallite size.

Table 4.5 ORR activity parameters of Pt-Pd/CX and the commercial Pt/C catalysts.

Catalysts	Onset potential / V vs RHE	Half-wave potential / V vs RHE	Current density / mA cm <sup>-2</sup>
Pt-Pd/CX-MeOH	0.883	0.629	6.46
Pt-Pd/CX-EtOH	0.792	0.570	4.00
Pt-Pd/CX-nPrOH	0.760	0.573	5.58
Pt-Pd/CX-FMY	0.785	0.656	6.65
Pt-Pd/CX-AA	0.756	0.543	5.00
Pt/C Alfa Aesar	0.885	0.717	7.04

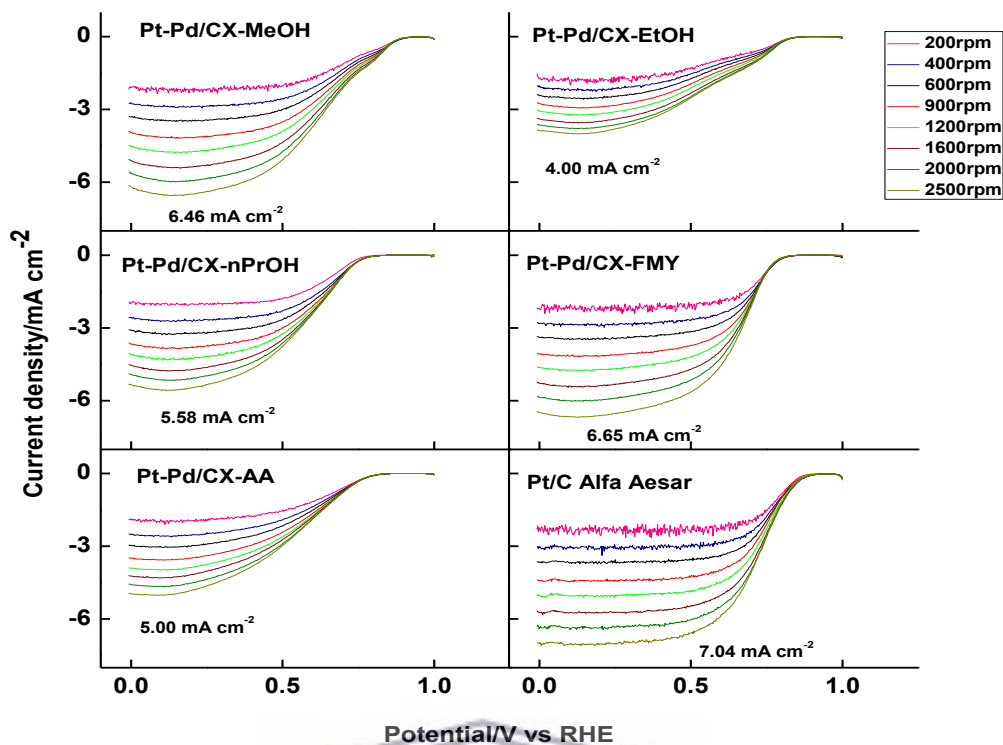


Figure 4.10-ORR polarisation curves recorded for the Pt-Pd/CX and the commercial Pt/C catalysts.

Figure 4.11 shows the current densities developed during the ORR performed on the catalysts supported on carbon black, while the Table 4.6 shows the most relevant activity parameters. Among the synthesised catalysts, Pt-Pd/CB-AA displayed the most positive onset (0.861 V) and half-wave potential (0.648 V) at 2500 rpm, whereas Pt-Pd/CB-FMY showed the less positive half wave potential. Furthermore, the highest diffusional current density at 2500 rpm was also recorded for Pt-Pd/CX-AA (6.98 mA cm<sup>-2</sup>), a value close to that of the commercial catalyst (7.04 mA cm<sup>-2</sup>). It is important to highlight that the synthesised Pt-Pd catalysts developed high diffusional current densities, considering their low Pt content compared to the commercial catalyst (see table 4.2).



Table 4.6 ORR activity parameters of Pt-Pd/CB and the commercial Pt/C catalysts.

Catalysts	Onset potential / V vs RHE	Half-wave potential / V vs RHE	Current density / mA cm <sup>-2</sup>
Pt-Pd/CB-MeOH	0.824	0.570	5.12
Pt-Pd/CB-EtOH	0.771	0.609	3.86
Pt-Pd/CB-nPrOH	0.824	0.612	6.43
Pt-Pd/CB-FMY	0.797	0.596	5.40
Pt-Pd/CB-AA	0.861	0.648	6.98
Pt/C Alfa Aesar	0.885	0.717	7.04

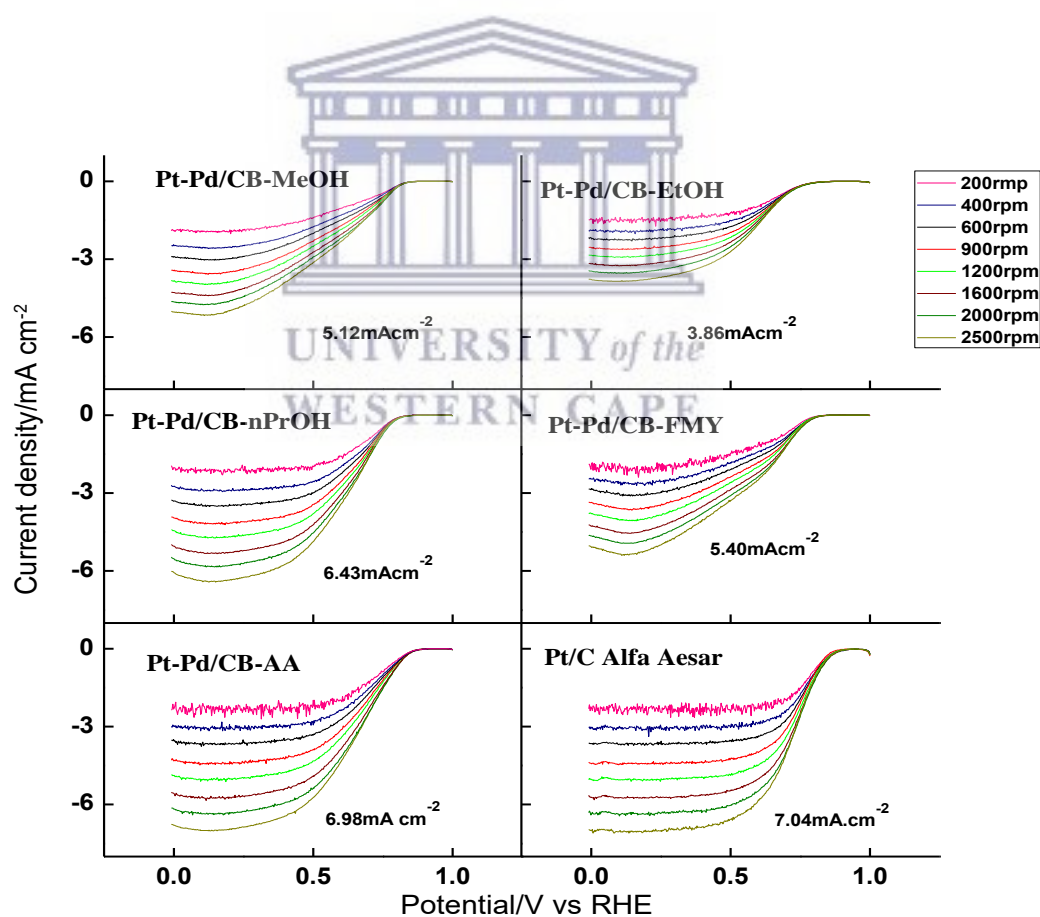


Figure 4.11- ORR polarisation curves recorded for the Pt-Pd/CB and the commercial Pt/C catalysts.



The ORR activities of the catalysts supported on carbon nanofibers are presented in Figure 4.12. Among the group of the synthesised catalysts, Pt-Pd/CNF-EtOH presented the most positive onset potential (0.827V), although the commercial catalyst displayed the highest onset potential (0.885V). Despite this result, it is important to highlight that the catalysts Pd/CNF-FMY and Pd/CNF-nPrOH developed the highest half-wave potentials, while the catalyst Pd/CNF-EtOH developed the highest diffusional current density (6.51 mA cm<sup>-2</sup>) among the synthesised catalysts.

Table 4.7 ORR activity parameters of Pt-Pd/CNF and the commercial Pt/C catalysts.

Catalysts	Onset potential / V vs	Half-wave potential / V	Current density / mA cm <sup>-2</sup>
	RHE	vs RHE	
Pt-Pd/CNF-MeOH	0.773	0.458	4.10
Pt-Pd/CNF-EtOH	0.827	0.639	6.51
Pt-Pd/CNF-nPrOH	0.819	0.651	6.08
Pt-Pd/CNF-FMY	0.619	0.453	5.13
Pt-Pd/CNF-AA	0.651	0.470	3.93
Pt/C Alfa Aesar	0.885	0.717	7.04

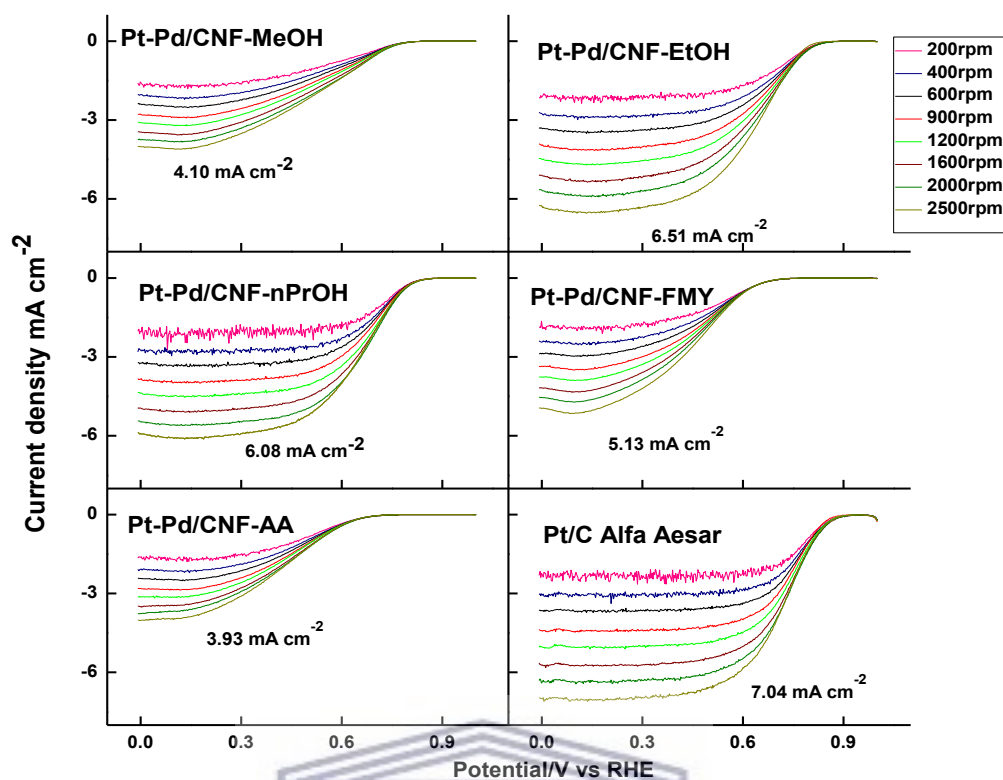


Figure 4.12- ORR polarisation curves recorded for the Pt-Pd/CNF and the commercial Pt/C catalysts.

#### 4.2.3 Mass and specific activity of the synthesised catalysts.

The specific and mass activities of the catalysts supported on carbon xerogels at 0.75 V were calculated and the results are depicted in the Figure 4.13. The catalysts reduced with methanol, ethanol and formaldehyde displayed the highest mass and specific activities, even overcoming those of Pt/C, while the catalyst reduced with ascorbic acid generated the lower activities. These results confirm that the Pt-Pd/CX materials are suitable to be used in the cathode of the PEMFCs as they have a low but optimized Pt content, high content of active sites and high activity toward the ORR. The higher lattice parameter matched with the higher activity of the catalysts, suggesting that a low alloying degree between Pt and Pd benefits their activity.

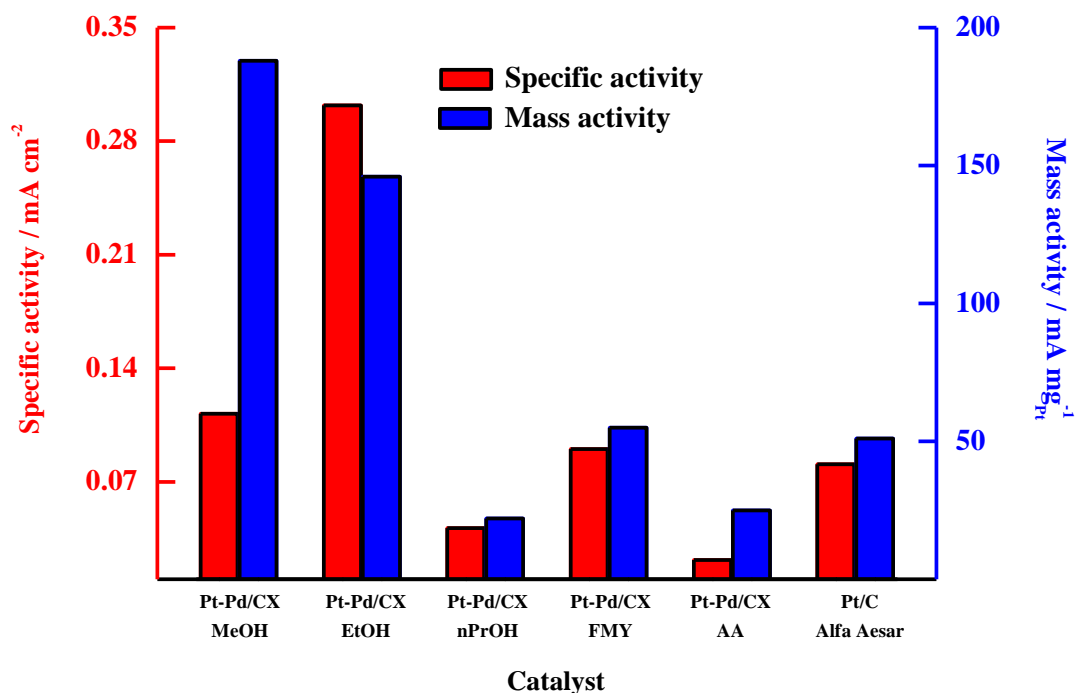


Figure 4.13 Specific and mass activities of the Pt-Pd/CX and the commercial Pt/C catalysts.

Figure 4.14 displays the mass and specific activity of the catalysts supported on carbon black. The catalyst with the highest mass activity is Pt-Pd/CB-AA and the lowest was generated by Pt-Pd/CB-EtOH. The catalysts reduced with ethanol presented both the lowest mass and specific activities, which was also demonstrated with their lowest diffusional current densities. The activities observed in the catalysts supported on carbon black were comparatively lower than those of the catalysts supported on carbon xerogels, a fact that can be explained from the high content of mesopores in the carbon xerogels. A high content of mesopores promotes a high dispersion of metal nanoparticles on the carbon support, and the diffusion of the electroactive species toward the catalytic nanoparticles.

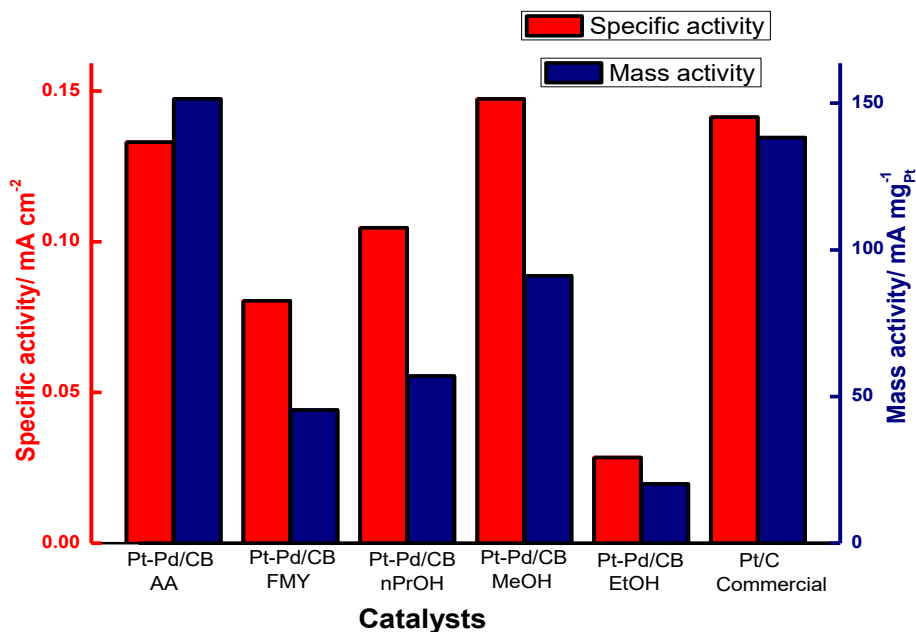


Figure 4.14 Specific and mass activities of the Pt-Pd/CB and the commercial Pt/C catalysts.

Figure 4.15 shows the results for the specific and mass activities of the catalysts supported on carbon nanofibers. Pt-Pd/CNF-nPrOH developed the highest specific activity, even overcoming that of Pt/C, while Pt-Pd/CNF-EtOH developed the highest mass activity compared to the other CNF-supported materials. The mass and specific activities of the catalysts reduced with ascorbic acid and formaldehyde were lower than those of the catalysts. The catalysts supported on carbon nanofibers did not achieve the expected 40 wt. % metal content (see table 4.3) which results in their low activity among all the studied materials in this work. Therefore, the low metal content of the catalysts supported on carbon nanofibers could be the main reason related with the low mass and specific activities of the Pt-Pd/CNF catalysts.

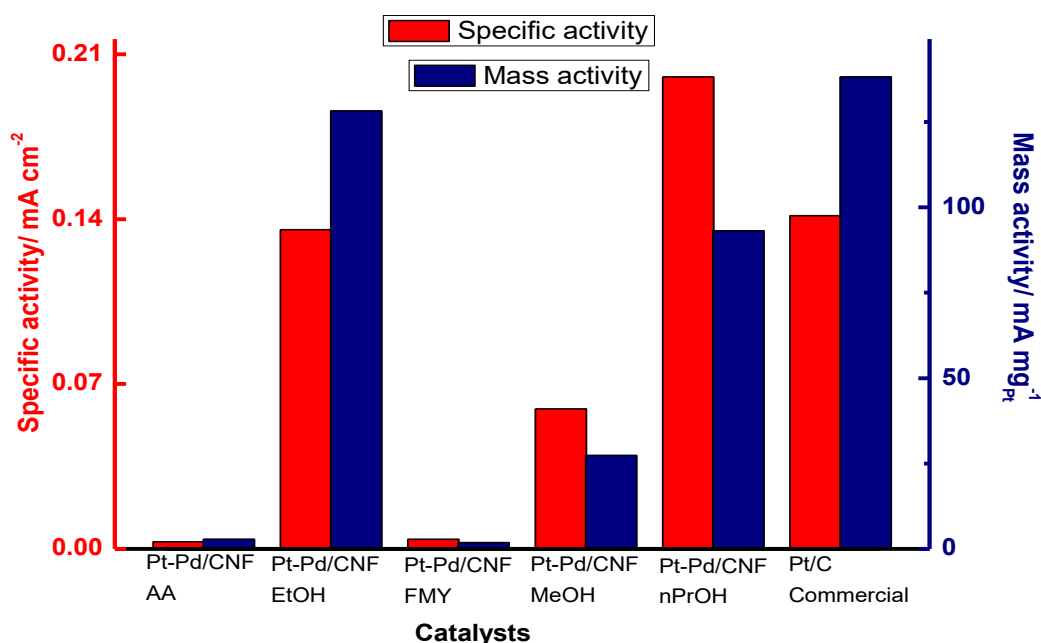


Figure 4.15 Specific and mass activities of the Pt-Pd/CNF and the commercial Pt/C catalysts.

#### 4.2.4 Koutecký-Levich analysis of the synthesised catalysts

Figure 4.16 shows the Koutecký-Levich plots at different potentials of the catalysts supported on carbon xerogels, which were used to calculate the number of electrons involved in the oxygen reduction reaction on the synthesised catalysts supported on carbon xerogels. The number of electrons was calculated using the Koutecký-Levich equation:

$$\frac{1}{I} = \frac{1}{I_k} + \frac{1}{0.62nFD^{2/3}\nu^{-1/6}C_{O_2}A\omega^{1/2}} \quad (4.4)$$

Where  $D$  is the diffusion coefficient of molecular oxygen in 0.1 M HClO<sub>4</sub> ( $1.67 \times 10^{-5} \text{ cm}^2 \text{ s}^{-1}$ ),  $\nu$  is the kinematical viscosity ( $8.93 \times 10^{-3} \text{ cm}^2 \text{ s}^{-1}$ ),  $C_{O_2}$  is the concentration of dissolved molecular oxygen ( $1.18 \times 10^{-6} \text{ mol cm}^{-3}$ ) and  $A$  is the geometric area of the working electrode ( $0.1962 \text{ cm}^2$ ). Parallel trends were found at the different potentials, suggesting that water is formed as the main product during the ORR. Pt-Pd/CX-EtOH is the only catalyst that presented a slight deviation from parallelism, indicating the formation of some hydrogen

peroxide during the ORR. The slopes of these linear trends were used to calculate the number of electrons, finding values close to four electrons, except in the case of the catalyst reduced with ethanol (3.7 electrons), demonstrating an incipient formation of hydrogen peroxide when the ORR is performed on this catalyst.

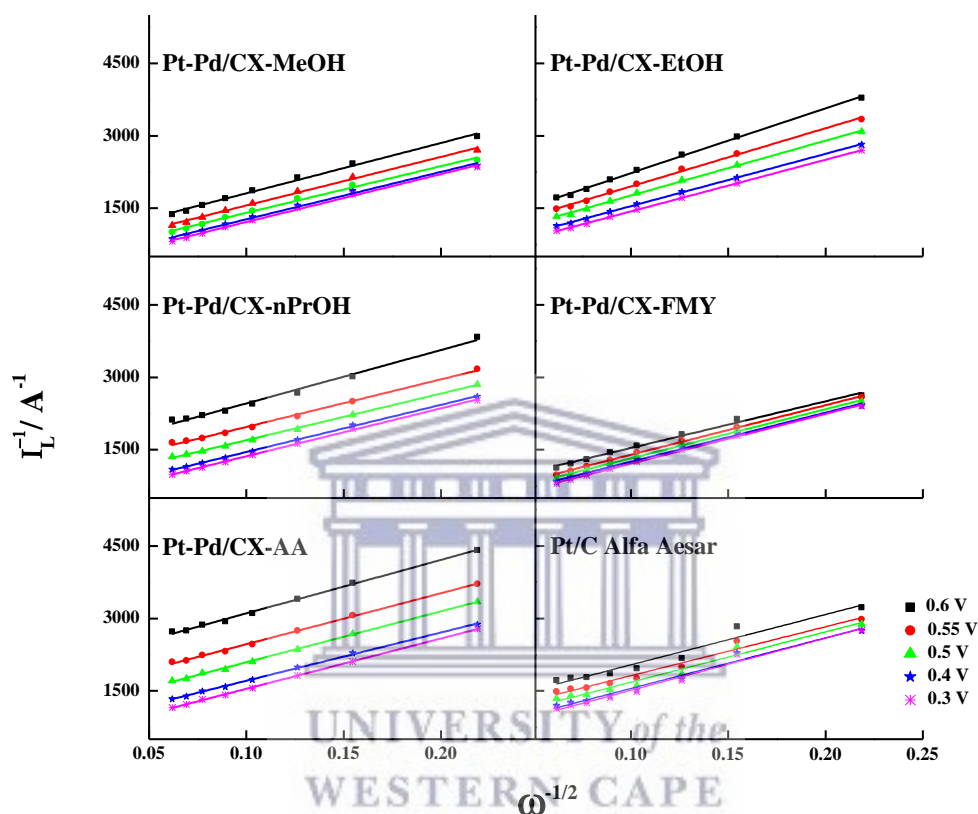


Figure 4.16 Koutecký-Levich plots of the Pt-Pd/CX and the commercial Pt/C catalysts.

Regarding the catalysts supported on carbon black, the materials Pt-Pd/CB-AA, Pt-Pd/CB-FMY and Pt-Pd/CB-nPrOH presented four number of electrons involved in the ORR, indicating the formation of water as main product. The catalysts Pt-Pd/CB-EtOH and Pt-Pd/CB-MeOH showed a number of electrons lower than four (3.1 and 3.2 respectively), suggesting that some hydrogen peroxide is formed when the ORR occurs on these materials. The catalysts reduced with ethanol supported on both carbon xerogel and carbon black involved less than four electrons, indicating that this synthesis route does not promote the

formation of nanoparticles with catalytic properties favouring the production of water [12, 13].

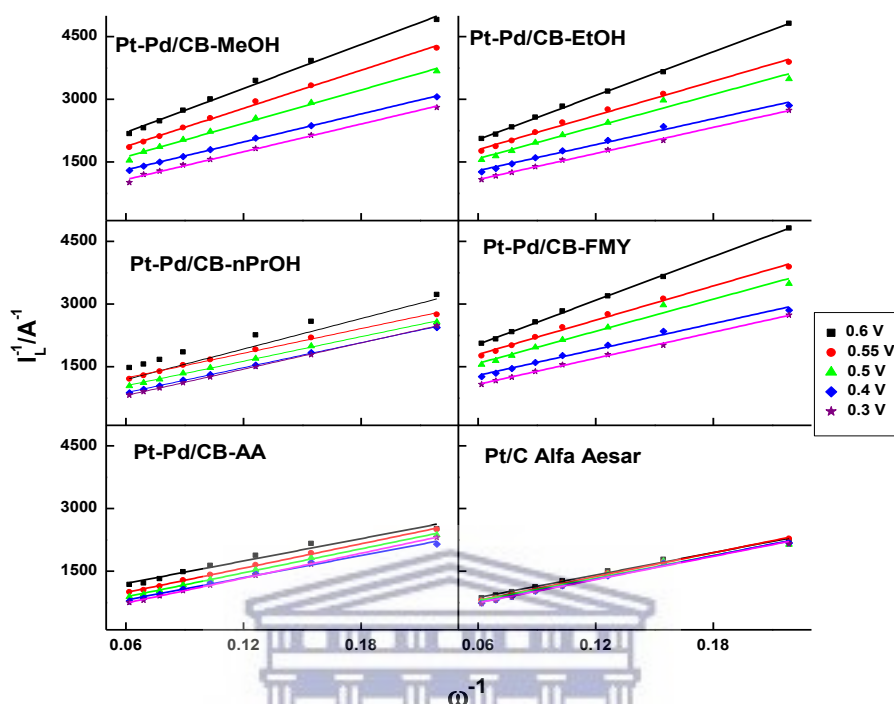


Figure 4.17 Koutecký-Levich plots of the Pt-Pd/CB and the commercial Pt/C catalysts.

In the case of the materials supported on carbon nanofibers, parallel trends were observed (see Figure 4.18) in the catalysts reduced with ethanol (4.1 electrons), *n*-propanol (4.3 electrons) and formaldehyde (4.3 electrons), suggesting the formation of water as main product. The catalysts reduced with ascorbic acid and methanol showed a number of electrons lower than four (3.2 and 3.1 electrons respectively), suggesting some hydrogen peroxide formation.

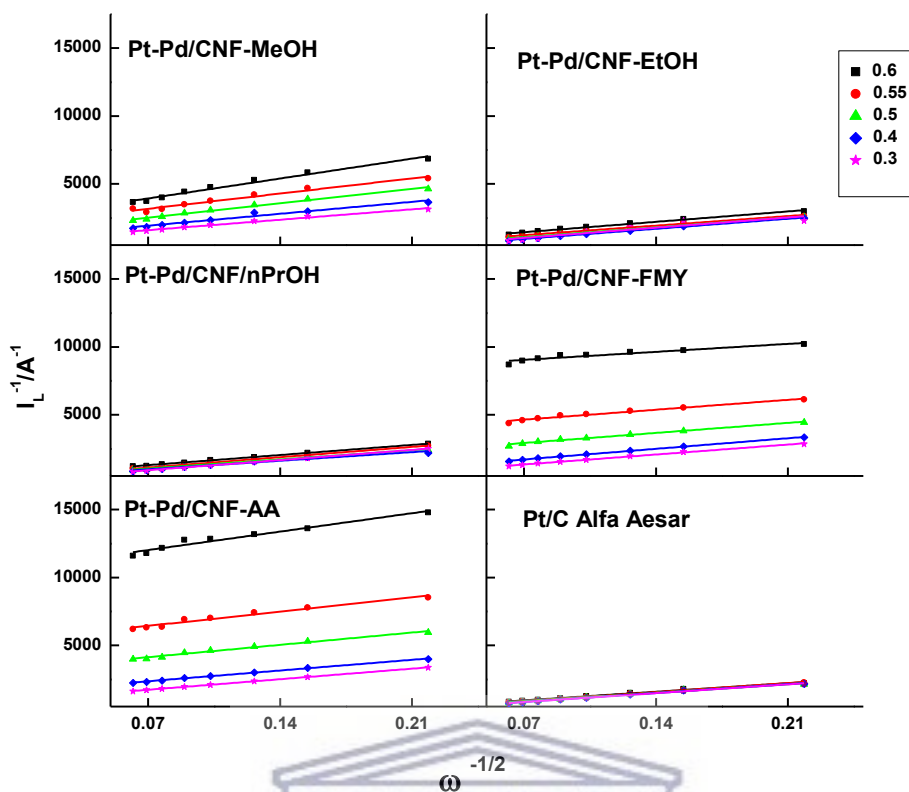


Figure 4.18 Koutecký-Levich plots of the Pt-Pd/CNF and the commercial Pt/C catalysts.

#### 4.2.5 Corrosion and stability assessment of the synthesised catalysts.

The synthesised catalysts were tested to assess the corrosion resistance in similar conditions to those employed in a PEMFC, following the procedure described in section 3.1.3.2. The changes in the electrochemical behaviours of the catalysts supported on carbon xerogels are presented in Figure 4.19. A negligible change in the peaks corresponding to hydrogen adsorption/desorption current densities (between -0.1 to 0.3 V vs RHE) with well-defined peaks for adsorption was observed, which indicates that there was no changes in the surface crystallinity of the nanoparticles. Pt-Pd/CX-FMY demonstrated a decrease in the current densities of the peaks corresponding to formation/reduction of metal oxides (between 0.6 to 0.95 V vs RHE), suggesting the formation of unstable surface oxides. No other synthesised catalysts showed significant changes after the cycling test suggesting high resistance towards corrosion.



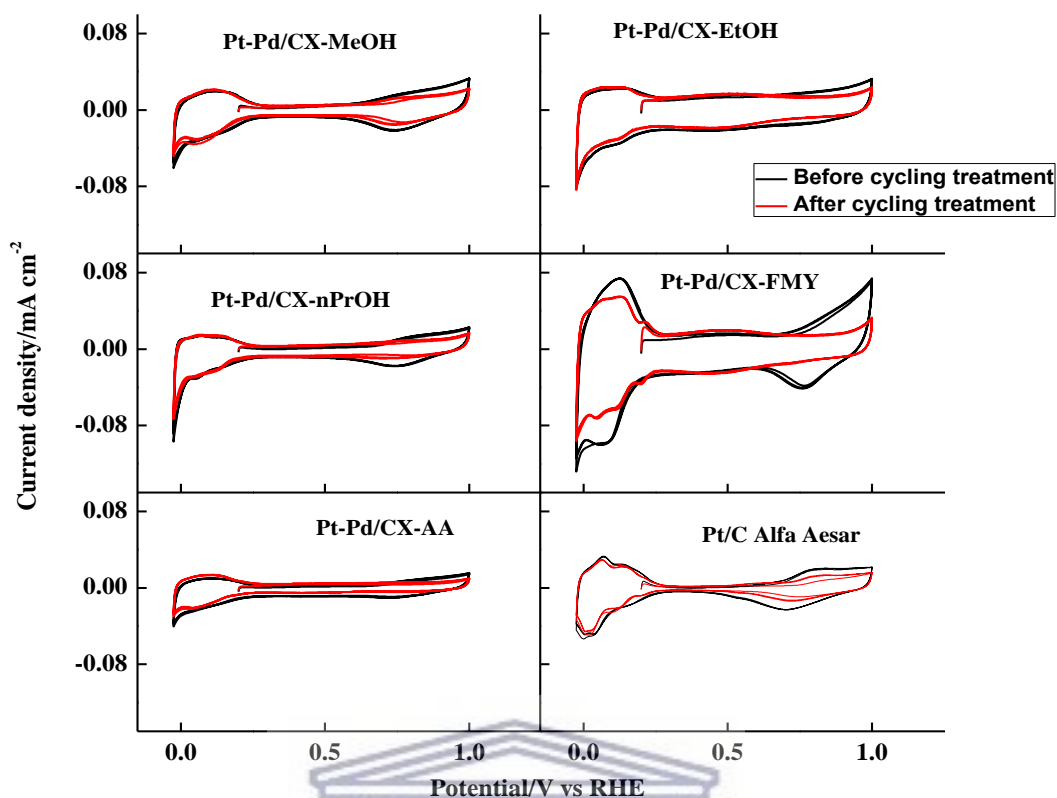


Figure 4.19 Cyclic voltammograms of Pt-Pd/CX and the commercial Pt/C catalysts before and after the cycling treatment.

The synthesised catalysts supported on carbon black demonstrated changes in the peaks corresponding to the adsorption and desorption of hydrogen after the cycling treatment, except in the case of the catalyst reduced with methanol. The peaks corresponding to the oxidation/reduction of metal oxides changed drastically in all the synthesised catalyst, which means a dissolution process of the metal nanoparticles [14]. The catalysts Pt-Pd/CX displayed higher stability and resistance to corrosion compared with the catalysts Pt-Pd/CB, verifying that carbon xerogel have improved corrosion resistance in acidic media.

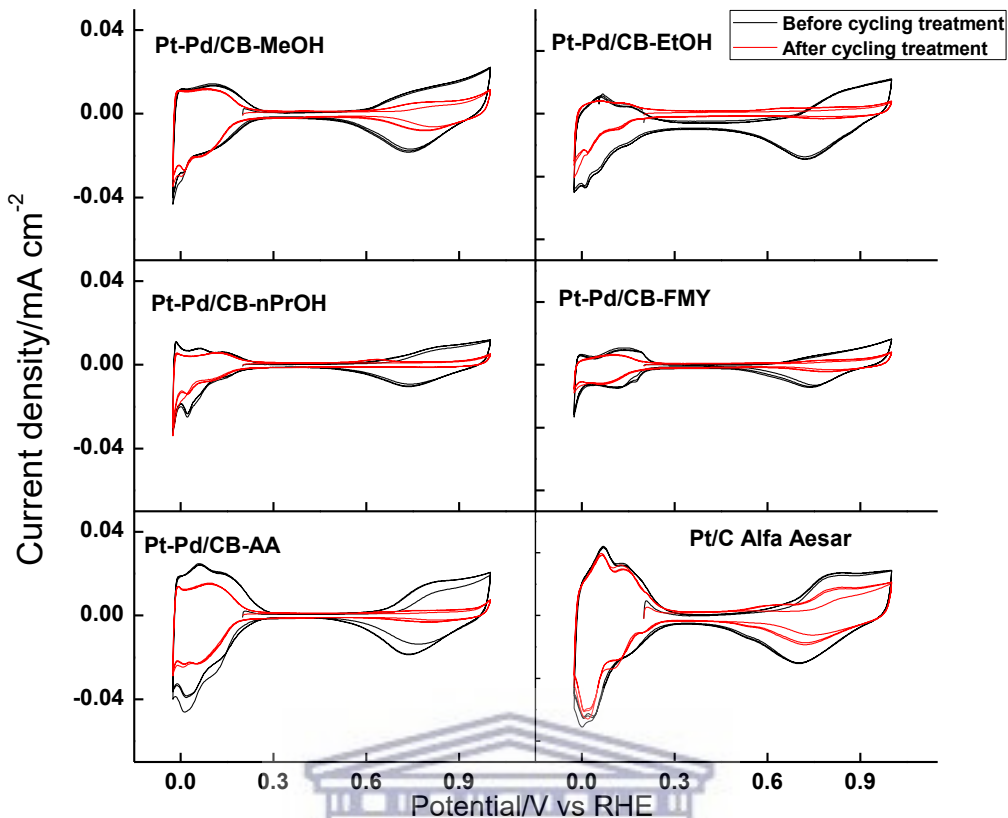


Figure 4.20 Cyclic voltammograms of Pt-Pd/CB and the commercial Pt/C catalysts before and after the cycling treatment.

Figure 4.21 depicts the behaviour of the catalysts supported on carbon nanofibers in the O<sub>2</sub>-free supporting electrolyte, before and after the durability test. Only the catalyst reduced with ethanol did not show a change in the current density corresponding to the adsorption/desorption of hydrogen, suggesting that there was no change on the crystallinity of this material. There were changes in the current densities corresponding to the formation/reduction of metal oxides in the other synthesised catalysts, indicating that they are more sensible to corrosion processes associated with both, the metal nanoparticles and carbon support corrosion.

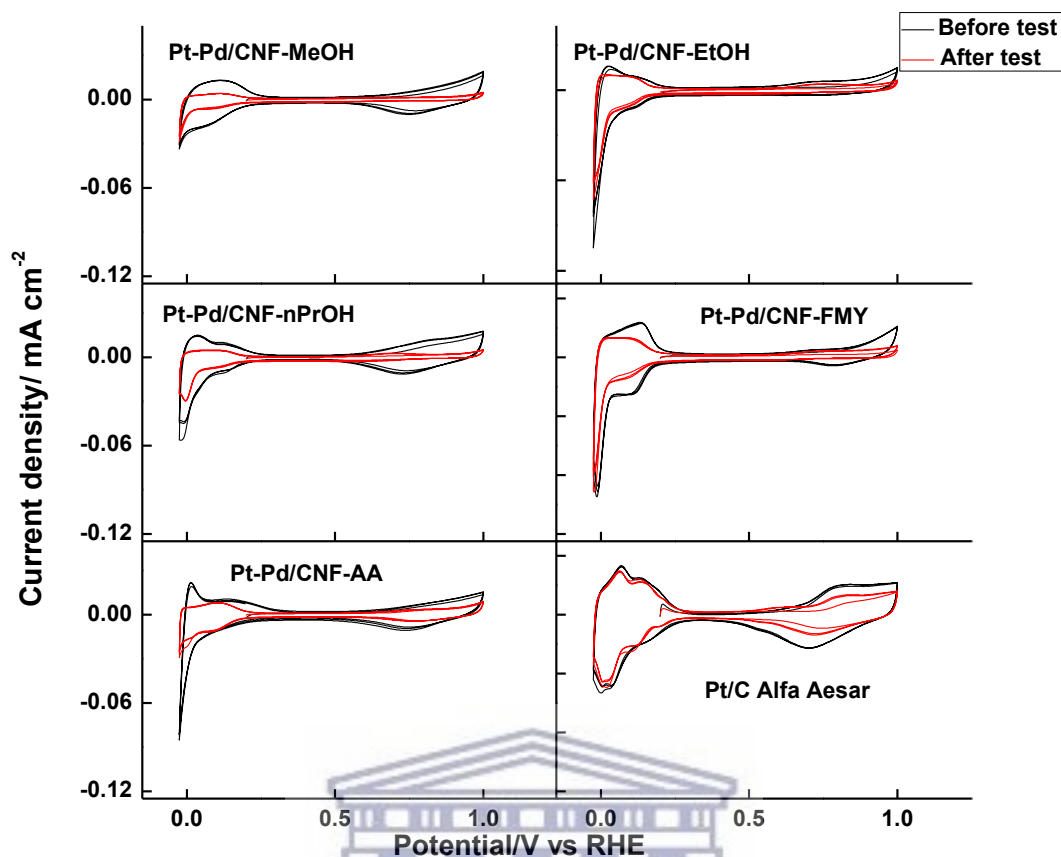


Figure 4.21 Cyclic voltammograms of Pt-Pd/CNF and the commercial Pt/C catalysts before and after the cycling treatment.

The effect of the cycling treatment in the ORR activity was also studied on the catalysts supported on carbon xerogels, as shown in Figure 4.22. There is a shift toward more negative values in the half-wave potentials after the cycling treatment although the diffusional current densities increased after the test, indicating that the corrosion of the catalysts is mainly associated to the carbon support and thus, an increase in the electroactive area is generated. All the Pt-Pd materials showed lower differences in the half-wave potential than that of the commercial Pt/C, indicating that synthesised Pt-Pd/CX materials possess a high corrosion resistance, which can be attributed to the presence of both Pd and carbon xerogels. These

results were in consistence with those achieved by Nishanth [15] and Xiong [16], who found small differences in the half-wave potentials before and after the durability test, for materials prepared by galvanic replacement and solvothermal synthesis.

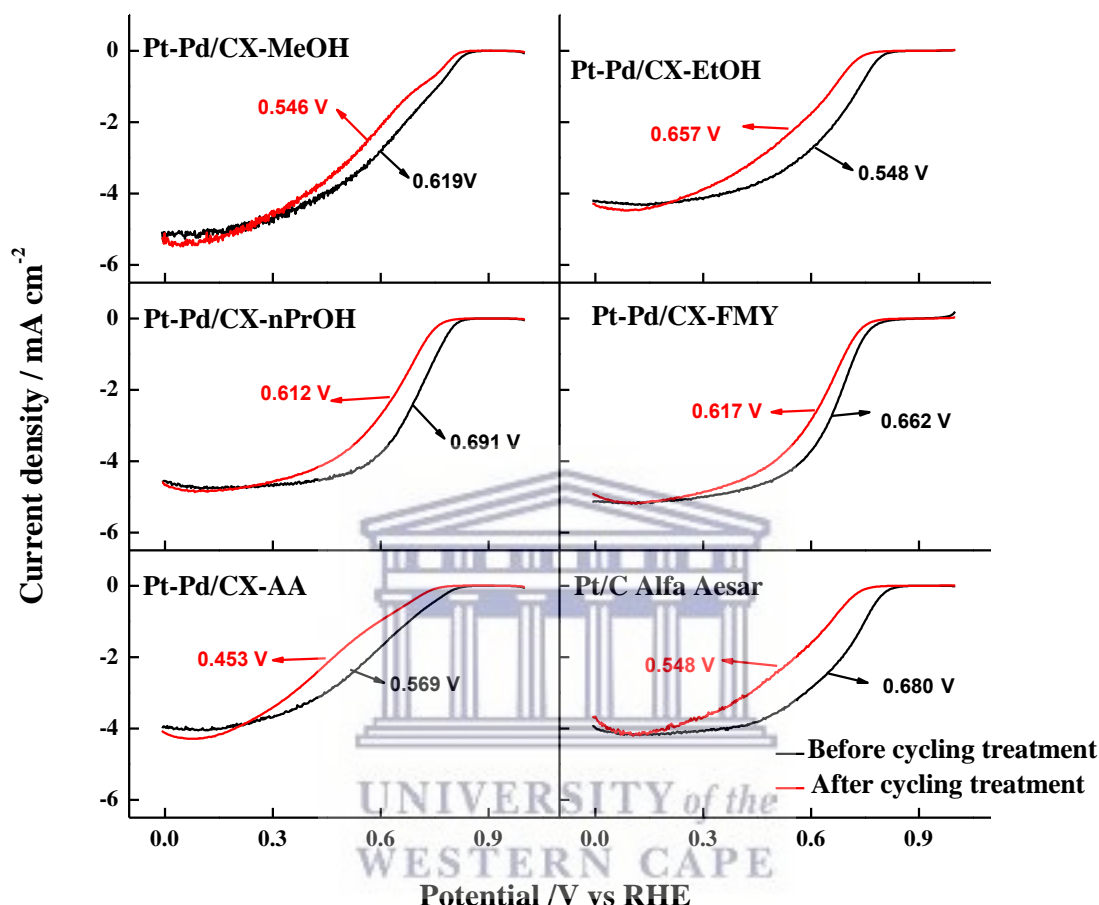


Figure 4.22 ORR polarisation curves recorded at 1600 rpm for the Pt-Pd/CX and the commercial Pt/C catalysts before and after the cycling treatment.

Figure 4.23 shows the effect of the cycling treatment on the activity of the catalysts supported on carbon black. The half-wave potentials of the catalysts decreased drastically in the prepared materials compared with the commercial Pt/C, except in the case of Pt-Pd/CB-FMY and Pt-Pd/CB-MeOH. The diffusional current densities were also affected, since all of them decreased after the cycling, suggesting corrosion processes affecting both the carbon black support and the metal Pt-Pd nanoparticles.

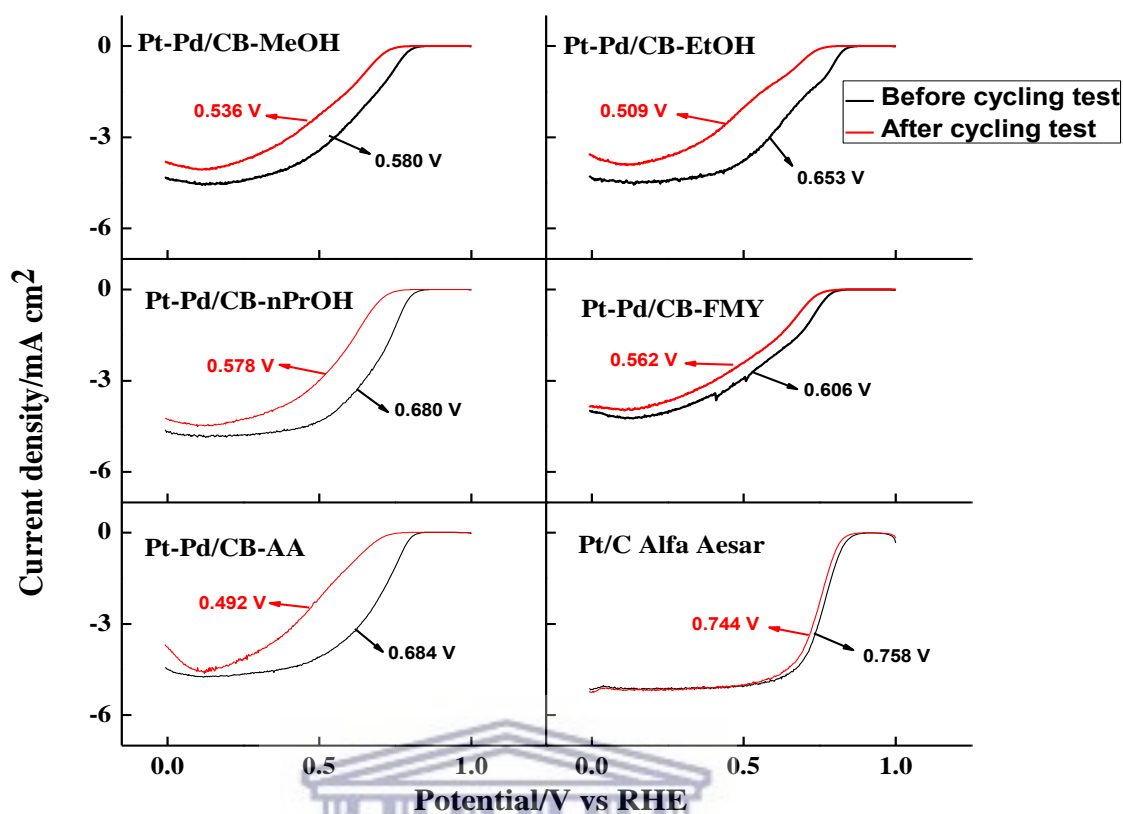


Figure 4.23 ORR polarisation curves recorded at 1600 rpm for the Pt-Pd/CB and the commercial Pt/C catalysts before and after the cycling treatment.

Figure 4.24 represents the performance of the ORR on the Pt-Pd/CNF catalysts. The half-wave potential of the catalyst reduced with ascorbic acid presented the smallest change compared to the other synthesised catalysts, which means this material develops the lowest degree of corrosion. Moreover, among all the catalysts supported on the different carbon materials, the highest decrease in the half-wave potential was recorded on Pt-Pd/CB-AA and the lower on Pt-Pd/CB-MeOH.

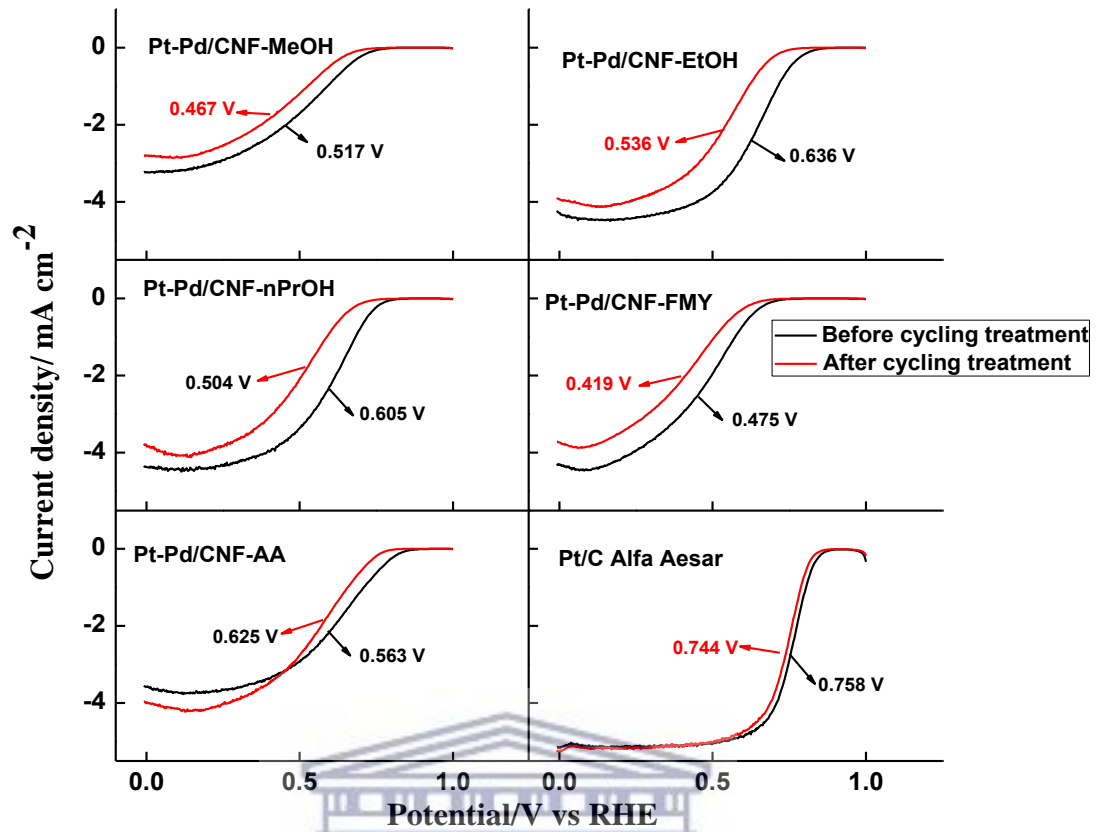


Figure 4.24 ORR polarisation curves recorded at 1600 rpm for the Pt-Pd/CB and the commercial Pt/C catalysts before and after the cycling treatment.

## References

1. Góral-Kurbiel, M., Kosydar, R., Gurgul, J., Dembińska, B., Kulesza, P.J. and Drelinkiewicz, A., 2016. Carbon supported Pd<sub>x</sub>Pt<sub>y</sub> nanoparticles for oxygen reduction. The effect of Pd: Pt ratio. *Electrochimica Acta*, 222, pp.1220-1233.
2. Calderón, J.C., Mahata, N., Pereira, M.F.R., Figueiredo, J.L., Fernandes, V.R., Rangel, C.M., Calvillo, L., Lázaro, M.J. and Pastor, E., 2012. Pt–Ru catalysts supported on carbon xerogels for PEM fuel cells. *international journal of hydrogen energy*, 37(8), pp.7200-7211.
3. Kadirgan, F., Kannan, A.M., Atilan, T., Beyhan, S., Ozenler, S.S., Suzer, S. and Yörür, A., 2009. Carbon supported nano-sized Pt–Pd and Pt–Co electrocatalysts for proton exchange membrane fuel cells. *international journal of hydrogen energy*, 34(23), pp.9450-9460.
4. Lopes, T., Antolini, E. and Gonzalez, E.R., 2008. Carbon supported Pt–Pd alloy as an ethanol tolerant oxygen reduction electrocatalyst for direct ethanol fuel cells. *international journal of hydrogen energy*, 33(20), pp.5563-5570.
5. Calderón, J.C., García, G., Calvillo, L., Rodríguez, J.L., Lázaro, M.J. and Pastor, E., 2015. Electrochemical oxidation of CO and methanol on Pt–Ru catalysts supported on carbon nanofibers: The influence of synthesis method. *Applied Catalysis B: Environmental*, 165, pp.676-686.
6. Caruso RA, Ashokkumar M, Grieser F. Sonochemical formation of colloidal platinum. *Colloids Surf A* 2000;169:219-25.
7. Wang, X. and Hsing, I.M., 2002. Surfactant stabilized Pt and Pt alloy electrocatalyst for polymer electrolyte fuel cells. *Electrochimica acta*, 47(18), pp.2981-2987.

8. Hui, C.L., Li, X.G. and Hsing, I.M., 2005. Well-dispersed surfactant-stabilized Pt/C nanocatalysts for fuel cell application: Dispersion control and surfactant removal. *Electrochimica acta*, 51(4), pp.711-719.
9. Muntean, R., Rost, U., Marginean, G. and Vaszilcsin, N., 2015, March. Determination of the electrochemical surface area for CNTs-PT electro catalyst using cyclic voltammetry. In *Proceedings of 9th International Conference on Materials Science and Engineering–BRAMAT*.
10. Li, H., Sun, G., Li, N., Sun, S., Su, D. and Xin, Q., 2007. Design and preparation of highly active Pt–Pd/C catalyst for the oxygen reduction reaction. *The Journal of Physical Chemistry C*, 111(15), pp.5605-5617.
11. Qin, Y.H., Yang, H.H., Zhang, X.S., Li, P. and Ma, C.A., 2010. Effect of carbon nanofibers microstructure on electrocatalytic activities of Pd electrocatalysts for ethanol oxidation in alkaline medium. *International Journal of Hydrogen Energy*, 35(15), pp.7667-7674.
12. Lopes, T., Antolini, E. and Gonzalez, E.R., 2008. Carbon supported Pt–Pd alloy as an ethanol tolerant oxygen reduction electrocatalyst for direct ethanol fuel cells. *international journal of hydrogen energy*, 33(20), pp.5563-5570.
13. Al-Azri, Z.H., Chen, W.T., Chan, A., Jovic, V., Ina, T., Idriss, H. and Waterhouse, G.I., 2015. The roles of metal co-catalysts and reaction media in photocatalytic hydrogen production: Performance evaluation of M/TiO<sub>2</sub> photocatalysts (M= Pd, Pt, Au) in different alcohol–water mixtures. *Journal of Catalysis*, 329, pp.355-367.
14. Calderón, J.C., Ndzuzo, L., Bladergroen, B.J. and Pasupathi, S., 2018. Oxygen reduction reaction on Pt-Pd catalysts supported on carbon xerogels: Effect of the synthesis method. *International Journal of Hydrogen Energy*.



15. Nishanth, K.G., Sridhar, P. and Pitchumani, S., 2013. Carbon-supported Pt encapsulated Pd nanostructure as methanol-tolerant oxygen reduction electro-catalyst. *international journal of hydrogen energy*, 38(1), pp.612-619.
16. Xiong, X., Chen, W., Wang, W., Li, J. and Chen, S., 2017. Pt-Pd nanodendrites as oxygen reduction catalyst in polymer-electrolyte-membrane fuel cell. *International Journal of Hydrogen Energy*, 42(40), pp.25234-25243.



## 5. Chapter Five: Conclusions

Platinum-palladium catalysts supported on carbon xerogels, carbon black and carbon nanofibers were synthesised by chemical reduction with methanol, ethanol, *n*-propanol, formaldehyde and ascorbic acid, in order to evaluate their performance toward the oxygen reduction reaction (ORR) and thus determining its suitability as cathode catalysts for PEMFCs. The catalysts were physically characterised by X-ray diffraction (XRD), energy dispersive X-ray (EDS) and transmission electron microscopy (TEM). Moreover, the as-synthesised materials were electrochemically characterised by cyclic voltammetry (CV) and rotating disk electrode (RDE). XRD analysis demonstrated the formation of an alloy between platinum and palladium, since the typical peaks of the face-centered structure of these catalysts shifted to the higher values of  $2\theta$  degrees, compared with the reflections of the commercial Pt/C catalyst. Furthermore, in most of the catalysts a decrease in the lattice parameter was found, verifying the entrance of Pd in the crystal lattice of Pt, forming an alloy. The EDS analysis showed that the Pt-Pd atomic ratio was close to 1:2 in the as-prepared catalysts, while the metal contents were around 35 wt. % for the catalysts supported on carbon xerogels, 36 wt. % for the catalysts supported on carbon black and 24 wt. % for the materials supported on carbon nanofibers. TEM analysis demonstrated a high dispersion of metal nanoparticles on the carbon supports, especially in the case of the Pt-Pd/CNF catalysts. Among the studied synthesis methods, the use of ethanol as reducing agent promoted a narrow particle size distribution of the nanoparticles on all the carbon supports.

Regarding the electrochemical characterisation, a shift towards more positive potentials in the peaks correspond to the reduction of metal oxides in the O<sub>2</sub>-free supporting electrolyte was observed due to the presence of Pd in the synthesised catalysts. Pt-Pd/CX-FMY, Pt-Pd/CX-MeOH, Pt-Pd/CB-AA, Pt-Pd/CB-*n*PrOH, Pt-Pd/CNF-EtOH and Pt-Pd/CNF-*n*PrOH

demonstrated the highest activity towards the ORR, even overcoming the diffusional current densities developed by the commercial Pt/C Alfa Aesar catalyst. It is important to highlight that the materials synthesised in this work contain a lower platinum content and in most of the cases, they developed activities higher than that of Pt/C. After a Koutécy-Levich analysis of the catalysts, there were four electrons involved in the ORR found, suggesting the production of water as main product and the maximum efficiency of the catalysts. The mass and specific activity of the studied catalysts at 0.75 V was determined, and the obtained values demonstrated that Pt-Pd/CX-EtOH, Pt-Pd/CX-FMY and Pt-Pd/CX-MeOH possess activities higher than that of Pt/C. Pt-Pd/CX-AA and Pt-Pd/CNF-nPrOH also exhibited higher mass activities than that of Pt/C, as well as Pt-Pd/CB-MeOH displayed an improved specific activity.

The corrosion resistance of the studied materials was evaluated by submitting them to a potential cycling, which did not affect the peaks corresponding to the adsorption/desorption process of hydrogen in the catalysts supported on carbon xerogels, except Pt-Pd/CX-FMY. Nevertheless, in the catalysts supported on carbon black and carbon nanofibers, a decrease in the currents corresponding to this process was observed. The diffusional current densities of the catalysts supported on carbon xerogels and Pt-Pd/CNF-AA improved after the cycling treatment, suggesting a corrosion process associated to the metal nanoparticles dissolution. The results here presented suggest that the studied synthesis routes are suitable to produce Pt-Pd catalysts supported on carbon xerogels, carbon black and carbon nanofibers, procedures that allow the obtaining of materials with an optimised utilization of Pt. Despite the low content of this metal, there is no detriment in their ORR activity, making them good candidates to be employed as cathodes in proton exchange membrane fuel cells.

## Publications

The results from this study have been published in two high impact factor international journals and another paper has been submitted for publication.

1. Juan Carlos Calderon Gomez; Linathi Ndzuzo; Bernard J Bladergroen; Sivakumar Pasupathi. Oxygen reduction reaction on Pt-Pd catalysts supported on carbon xerogels: effect of the synthesis method. *International Journal of Hydrogen Energy*, 2018. In press
2. Juan Carlos Calderon Gomez; Linathi Ndzuzo; Bernard J Bladergroen; Sivakumar Pasupathi. Catalytic activity of carbon supported-Pt-Pd nanoparticles toward the oxygen reduction reaction. *Materials Today: Proceedings*. Elsevier, 2017. ISSN 2214-7853.
3. Juan Carlos Calderon Gomez; Linathi Ndzuzo; Bernard J Baldergoen; Sivarkumar Pasupathi. Effect of different reducing agents in the performance of Pt-Pd catalysts supported on carbon black towards oxygen reduction reaction. *International Journal of Hydrogen Energy*, Special Issue "h2fc2018Trondheim (Pollet)". Submitted 31 December 2018.